CHALMERS
UNIVERSITY OF TECHNOLOGY

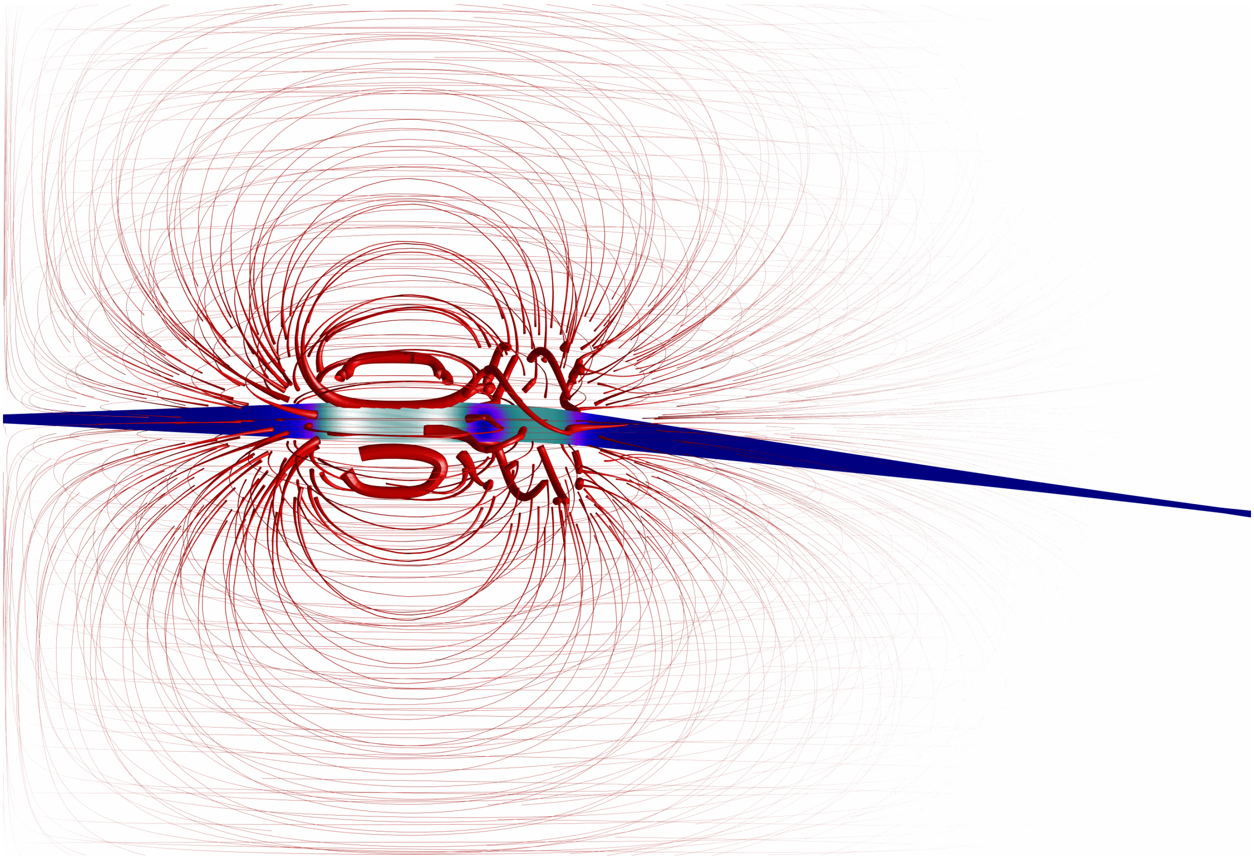

Modeling and Analysis of Aberrations in Electron Beam Melting (EBM) Systems

Master's thesis in Complex Adaptive Systems and Applied Physics

ARMIN AZHIRNIAN
DAVID SVENSSON

Department of Physics
CHALMERS UNIVERSITY OF TECHNOLOGY

Gothenburg, Sweden 2017

Master's thesis 2017

Modeling and Analysis of Aberrations in Electron Beam Melting (EBM) Systems

ARMIN AZHIRNIAN
DAVID SVENSSON

CHALMERS
UNIVERSITY OF TECHNOLOGY

Department of Physics
Division of Theoretical Physics
Chalmers University of Technology
Gothenburg, Sweden 2017

Modeling and Analysis of Aberrations in Electron Beam Melting (EBM) Systems
ARMIN AZHIRNIAN
DAVID SVENSSON

Supervisor: Christian Ekberg, Arcam AB
Examiner: Mattias Marklund, Department of Physics

Master's Thesis 2017
Department of Physics
Division of Theoretical Physics
Chalmers University of Technology
SE-412 96 Gothenburg
Telephone +46 31 772 1000

Cover: Magnetic field and electron beam trajectories in an Electron Beam Melting (EBM) system modeled using COMSOL Multiphysics®. The magnetic field lines are plotted in red, where the thickness of the line is proportional to the logarithm of the magnetic field magnitude. The color of the electron trajectories shows the magnitude of the Lorenz force acting on the electrons as the electron beam is focused and deflected.

Typeset in LaTeX
Gothenburg, Sweden 2017

Modeling and Analysis of Aberrations in Electron Beam Melting (EBM) Systems
ARMIN AZHIRNIAN
DAVID SVENSSON
Department of Physics
Chalmers University of Technology

Abstract

We present a modeling framework which can be used to study aberrations in an Electron Beam Melting (EBM) system. This is achieved by using COMSOL Multiphysics® software to model the magnetic fields and relativistic charged particle trajectories of a model EBM system. This involves defining a model for the magnetic lenses that handle the functions of focusing, deflecting and correcting the electron beam. Simulations of the magnetic fields have been made for multipole fields up to 24 poles. Methods have been developed for characterization and quantification of the beam in the model. This is done in terms of deflection angles, focusing power and aberration spectra. A realization of aberration correction using a superposition of a Quadrupole and a Hexapole in a single lens is also presented along with aberration coefficients. We conclude with a discussion of the practical implementation of the beam sensing and control in EBM and future use of the modeling tools built for this thesis.

Keywords: Electron Beam Melting, Electron Optics, Aberrations, Finite Element Method, Charged Particle Tracing, Magnetostatics

Acknowledgements

We would like to thank Christian Ekberg, Marie Doverbo and the rest of the people at Arcam AB for their support and inspiration. Our examiner Mattias Marklund has been very helpful as well. We are also thankful to the authors who happened to choose the most relevant chapters of their books to distribute as free samples. Finally we have greatly appreciated the enduring patience of the COMSOL support.

Armin Azhirnian and David Svensson, Gothenburg, June 2017

Contents

Chapter 1

Introduction

The Arcam electron beam melting (EBM) system uses a series of magnetic coil lenses to focus, deflect and shape an electron beam which melts metal powder in a precisely controlled pattern. A solid understanding of how perturbations and non-ideal conditions affect a system's reliability and performance is essential. This is particularly true when the system process involves non-linear interactions between the different parts of the system. This report describes how the COMSOL Multiphysics® software [1] can be used to model the aberrations in an EBM system. There is also a description of how the aberrations can be quantified and analyzed with the purpose of mitigating the effect of the aberrations.

A brief introduction to the EBM technology as well as the purpose and scope of this project is provided in this chapter. Chapter 2 starts with a short primer on the subjects of electron optics and aberrations in optical systems. The different types of magnetic lenses used in electron optical systems and the induced magnetic fields are also described in chapter 2. The chapter concludes with an introduction to the Finite Element Method (FEM) which is used to solve for the magnetic fields and electron trajectories.

Chapter 3 gives a detailed account of the methods that were used used in this project. There is also a section dedicated to the how the data from the model was analyzed. Results are presented in chapter 4. The report is concluded in chapter 5 in which the model, the results and suggestions for future work are discussed.

1.1 Background

For the last two decades, Arcam AB has developed a technique for additive manufacturing of metals using electron beam melting (EBM). Their products have gained particular success in the fields of medical implants and aerospace, where it has provided an alternative for conventional manufacturing. One of the major technical challenges of an EBM system is to accurately focus and steer the electron beam which then melts the metal in a precise pattern. This is achieved using a series of coils that generate magnetic fields which alter the trajectories of the electrons.

The inherent difficulties in designing optical elements for electron beams using magnetic coils has been known since the early work by Otto Scherzer, published in 1936 [2]. Aberrations are generated both from the geometry of the optical system and inhomogeneities in the induced magnetic fields. These aberrations will distort the electron beam spot which may affect the melting process. A robust aberration mitigation system is essential in ensuring a high reliability and consistency in the EBM process. This is especially important when the users of the EBM machine are part of industries with very strict specifications, such as the aerospace or the orthopedic industries.

1.2 Purpose

Additive manufacturing represents a disruptive technological development in many manufacturing industries. It allows the user to implement designs that would be difficult or even impossible to manufacture using conventional techniques. This opens up the possibilities of a new ways to design structures optimized to minimize the mass, cost, amount of material needed or fuel consumption in for instance aircraft [3].

The Arcam electron beam melting (EBM) process is used for additive manufacturing of metal components using a controllable electron beam to melt metal powder. The beam control system in Arcam's EBM machines consists of three magnetic lenses: the astigmatism lens, the focus lens and the deflection lens. This configuration is able to deflect the beam across the build area while maintaining a spot size of 140 µm to 250 µm, depending on the deflection angle. The spot diameter and shape is one of the major factors in the heating and melting of the metal. Accurate models and robust control of the spot size are therefore essential in order to ensure a stable process.

Many factors affect the resulting focus of the beam, but the angle between the optical axis and the electron trajectory is often the dominant factor. The challenge of ensuring a reliably focused spot becomes greater as the beam is deflected away from the optical axis. This limits further development of the EBM machines in two significant ways: the smallest spatial resolution of the builds and the largest deflection angle which determines the maximum size of the build.

A better understanding of the higher order aberrations and new ways to mitigate them would not only increase the reliability of the EBM machines currently in use but also enable the option to operate at a higher resolution or build size. Increasing the functionality and reliability of the EBM technology is an important step in the development of the additive manufacturing methods of the future.

1.3 Scope

The main goal of the project is to create a modeling framework with which aberrations in an electron beam melting system can be studied. The purpose of such a framework is to enable the user to make informed design decisions regarding both the minimization and mitigation of the aberrations. However, the short time frame of this project has meant that the number of specific cases which have been studied are limited.

The project began with a review of the available literature. However, most of the electron optic literature is written from the perspective of either electron microscopy or electron accelerators. From this we concluded that the models and theories used for electron microscopy were unsuited for the geometric scales of an EBM system. This resulted in a shift in the scope of the project; from applying existing model to a new problem to devolving a new model with knowledge from the old models.

Models and methods for analyzing and quantifying aberrations in an EBM system are required for a useful modeling framework. This was achived by repurposing methods used in electron microscopes for use in an EBM system. These methods depend are based on choosing an ideal beam for reference. We have limited the scope of our analysis to only include a small number of such references.

A part of the project is also dedicated to discussing the potential implementation and application of the created modeling framework. However, many of the potential cases which could be used to inform further study or future designs have not been modeled due to time constraints.

We have also chosen to limit the scope of the models on a technical level. Limits on the number of elements in a model are directly related to the amount of RAM on the modeling computer. Other limitations, such as keeping most of the dimensions in our model constant, are imposed in order to reduce the number of simulations needed in the parametric sweeps.

Chapter 2

Theory

Modeling the aberrations in an electron beam melting system requires not only an understanding of the trajectories of charged particles in an electromagnetic field but also knowledge of methods for solving the associated partial differential equations. While much previous work has been dedicated to solving this type of problem in other electron optical systems, such as electron microscopes, the results from the earlier work are not easily applicable in an EBM system. One of the most complete works in this field, *Principles of Electron Optics* by Hawkes and Kasper [4] provides a thorough description of the efforts made to understand and improve the performance of electron microscopes. However, a very detailed description of how aberrations are mitigated in electron microscopes are of limited use when modeling the aberrations in an EBM system. Therefore will we make no attempt to cover the entire topic in this chapter but instead to give the essential background for understanding and using the models presented in later chapters.

2.1 Electron Optics Introduction

Electron optics is a subset of the larger field of charged particle optics which describes how the trajectories of charged particles can be understood and manipulated. These manipulations are achieved by subjecting the charged particles to magnetic and electric fields which result in a force on the charged particle. Charged particle optical systems are often used to focus and steer beams of energetic charged particles. The beams have many applications such as electron microscopy, electron etching, ion beam deposition, and electron beam melting (EBM).

2.1.1 Brief history of electron microscopy

The first electron microscope was constructed by Ernst Ruska [5] and Max Knoll in 1931. While progress was initially slow, the inventors remained optimistic that they eventually would reach magnifications beyond the light based microscopes. Otto Scherzer [2] showed in 1936 that given a certain set of circumstances, magnetic lenses cannot be used in an electron optical system without introducing spherical and chromatic aberrations. This is one of the major differences from light based optics where a carefully designed lens can mitigate the spherical and chromatic aberrations. Unsuccessful attempts [6] to disprove Schertzer's theorem where made in the 1950s and 1960s.

The next forty years were spent trying to implement spherical aberration correctors based on violating one or many of the conditions for Schertzer's theorem. Hawkes [6] suggestes that the reason for the long period without any success was the difficulty of manufacturing the magnetic lenses with the required accuracy and stability.

Haider produced the first images using an aberration correction in a commercial TEM [7] in 1998. Since then, correctors based on a combinations of quadrupoles, hexapoles and octopoles have been implemented in a large number of electron microscopes. One of the prerequisites for this advancement was the availability of computers with sufficient computational power to control the correctors. The massive effort and work that it took to reach this level of correction is a consequence of the inherent difficulty of controlling electrons using electromagnetic fields. Peter W. Hawkes [6] summarizes the situation as:

> *"Electron lenses are extremely poor: if glass lenses were as bad, we should see as well with the naked eye as with a microscope!"*

2.1.2 Lorentz force

The Lorentz force is the force acting on a charged particle due to it moving in an electromagnetic field. The force on such a charged particle is given by

$$\mathbf{F} = q(\mathbf{v} \times \mathbf{B} + \mathbf{E}). \tag{2.1}$$

An electron optical system consists of one or a series of electromagnetic fields which perform an optical function such as focusing, deflection or aberration correction. While these fields are somewhat analogous to optical components such as lenses, there are fundamental differences in the function of optical and electron optical elements. The velocity dependence of the Lorentz force causes the beam to be refracted in an inhomogeneous and anisotropic way [8]. This results in a lens with chromatic aberration meaning that the optical power of the lens is proportional to the energy ("color") of the electron. The inevitability of spherical aberration [4] in an electromagnetic lens is another aspect of electron optics that differs from light based optics. The difficulty of correcting these aberrations has been and continues to be one of the major design drivers in the development of electron optical systems.

The use of the Lorentz force to drive an electron optical element is, however, not without advantages. The fact that the forces is proportional to both the velocity and charge of the particle allows mass or energy filters to be constructed. Another advantage is the speed at which a charged particle beam can be steered and focused. The overall speed of the optical elements is limited not by how fast a mirror or lens can be moved but by how fast a magnetic field can be altered.

2.1.3 Magnetic lenses

The force on a single particle is given by the Lorentz force (2.1) but how this force alters the shape and trajectory of an electron beam is not obvious. One of the

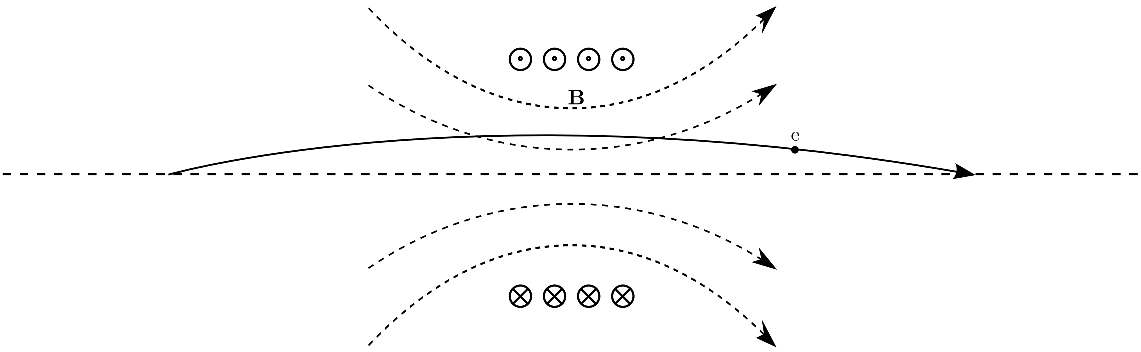

Figure 2.1: Simplified illustration of the trajectory of electron (solid line) passing through the magnetic field (dashed line) of a focusing lens coil. The initial velocity of the electron cannot be entirely parallel to the optical axis of the lens in order to have a resulting focusing effect. Note that the electron's helical rotation about the optical axis is not shown.

most important features of the magnetic component of the Lorentz force is that the direction of the force is perpendicular to both the velocity of the electron and the magnetic field. If there are no electric fields, the magnitude of Lorentz force can be rewritten as

$$F = evB\sin(\epsilon) \tag{2.2}$$

where ϵ is the angle between the direction of the magnetic field and the trajectory of the electron. A consequence of this is that no force is acting on an electron that moves parallel to the magnetic field.

Focusing lenses

A magnetic focus lens is a cylindrical lens made from a solenoid wound about the optical axis. The coil will induce a magnetic field that curves from the center of the coil but is parallel to the optical axis inside of the coil. A simplified illustration of a focusing coil is shown in figure 2.1. An electron that enters the coil with a velocity not entirely parallel to the magnetic field will be deflected back towards the optical axis. This condition is easily satisfied since the direction of the magnetic field changes direction along the optical axis. The only electrons that do not experience a focusing force are moving along and completely parallel to the optical axis. This type of magnetic focusing lens is both powerful in terms of of focusing power and how quickly it can be adjusted. The circular coil lens does however introduce aberrations and is by itself unable to produce a focused beam spot without so called spherical or chromatic aberrations. The nature and origin of these aberrations are discussed in section 2.2.

Multipole lenses

There are two primary uses for multipole lenses in an electron optical system: beam steering and aberration correction. The main difference between cylindrical magnetic focusing lenses and magnetic multipole lenses is that the magnetic fields of the multipole lenses are perpendicular to the optical axis. The magnetic force is given

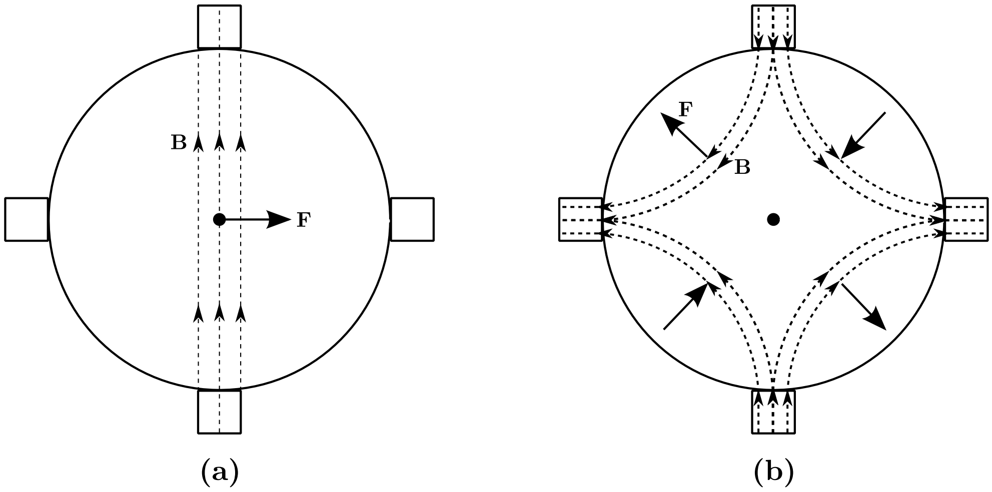

Figure 2.2: Cross section from **(a)** a deflection dipole and **(b)** a quadrupole stigmator showing the magnetic field and resulting forces on an electron moving out of the plane. The magnetic field is shown with dashed lines and the forces as solid arrows.

by the Lorentz force and is therefore perpendicular to both the magnetic field and the trajectory of the electrons.

A multipole lens is, as the name implies, composed of several magnetic poles placed in a circular arrangement with the optical axis in the center. The number of poles is almost exclusively chosen as an even number due to symmetry. Every pole is wound such that it has either the north or south pole pointing towards the optical axis. The function of the coil determines the configuration in terms of number of poles and the direction of the magnetic fields.

A deflection coil is used to deflect the electron beam and is composed of pairs of magnetic poles. These pairs are placed on opposite sides on a cylinder with the poles oriented in the same direction, as shown in figure (2.2a). It is common to design a deflection coil with two such pairs placed orthogonally to each other in order to allow any deflection angle in the X-Y plane.

An ideal deflection coil would have a perfectly homogeneous magnetic field with very short fall off regions along the optical axis. Deviations from this ideal implementation will cause aberrations in the electron beam. One of the most prominent aberrations is two-fold astigmatism. A a beam spot affected by this is elongated along some axis. A stigmator coil can be used to mitigate this effect.

A stigmator is a multipole coil with an even number of poles with an alternating field direction. An illustration of the magnetic field and Lorentz force of a quadrupole stigmator is shown in figure (2.2b). This stigmator would elongate the beam along one axis and push it together in the other axis. A single quadrupole stigmator can only pull apart or squeeze a beam along the two axes of the poles. A second quadrupole stigmator placed at an angle of $\pi/4$ radians to the first stigmator allows full rotation of the stigmator field. This principle can be applied to correct higher order of astigmatism. The angle between the two stigmators in such a corrector is

$$\theta = \frac{\pi}{2n} \tag{2.3}$$

where n is the order of symmetry that is being corrected. For example, third order astigmatism of any angle can be corrected by placing two hexapole stigmators at an angle of $\pi/6$ radians.

Limitations of Magnetic Lenses

It can be shown [9] that it impossible to build an electron optical focusing lens with negative focusing power using focusing coils. Another limitation is that magnetic fields cannot exert any work W on charged particles. This is seen by projecting the Lorentz force equation on the tangent $\mathrm{d}\mathbf{s}$ of the trajectories

$$W = \int q(\mathbf{v} \times \mathbf{B}) \cdot \mathrm{d}\mathbf{s}. \tag{2.4}$$

Since the tangent is proportional to the velocity

$$\mathbf{v} \cdot (\mathbf{v} \times \mathbf{B}) = (\mathbf{v} \times \mathbf{v}) \cdot \mathbf{B} \tag{2.5}$$

which means that the work must be equal to zero. From this we may conclude that we cannot increase nor decrease the energy of the charged particles with magnetic lenses. Thus we must depend on electrostatic fields for accelerating the electrons from rest.

2.2 Aberrations

An aberration is a deviation from an ideal optical system. The definitions of the different types of aberration vary between the different fields of study where the concept of aberrations is used. A common definition is based on measuring the phase difference of an aberrated wave-front compared to an ideal wave-front. The phase difference can then be projected onto an orthogonal polynomial basis where each basis vector corresponds to a certain type of aberration. The resulting aberration-spectrum is then used for quantification of the aberrations of the system.

The choice of the non-aberrated wavefront and the polynomial basis functions are made based on the optical system and the application of the aberration spectrum. The ideal wave front is often chosen as a plane wave focused onto a point when analyzing optical systems such as eyes or telescopes. It is also common to choose a polynomial basis in which convolutions can easily be expressed. This is because transforms between the optics and the image can often be expressed as convolution when the system operates close to the diffraction limit.

2.2.1 In Optics

The analysis of aberrations has many applications in optical systems where the aberration spectra can be used to quantify and correct an error in the optical system. Reducing the atmospheric noise in optical astronomy using adaptive optics [10] is an example of such an application. Another application is to use the aberration spectrum of the patient's eye to aid the diagnosis of certain eye disorders [11].

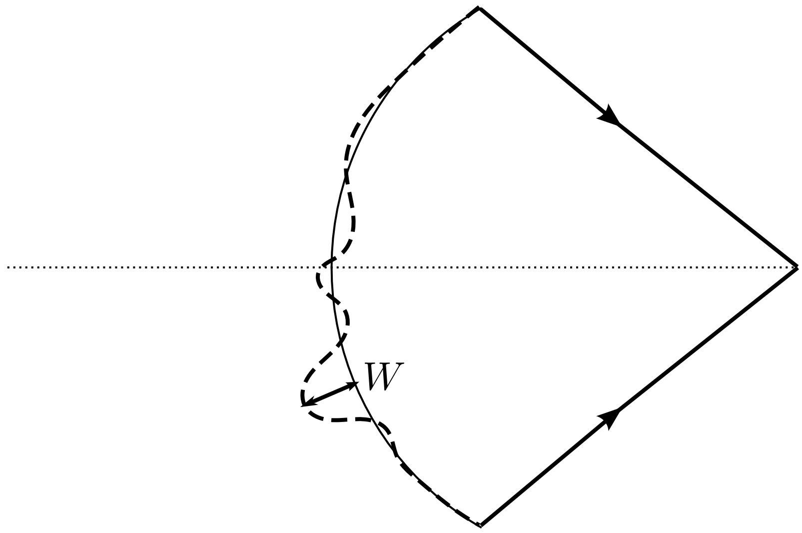

Figure 2.3: Illustration of the aberration function W which is equal to the difference between an ideal and an aberrated wave front. The aberrated wave front is illustrated as a dashed line and the optical axis as a dotted line. The ideal wave front here represents a wave that will be at a perfect focus at the right side of the figure.

Gaussian optics describes the concept of perfect focusing lenses that map plane waves propagating along an optical axis $\hat{z}$ to spherical waves converging at some focal point on that same axis. This ideal lens is used as a reference and the distance of the resulting wavefront from the ideal wavefront is defined as the error. Typically the error W is a scalar field in two dimensions that is converted to phase representation called the wave aberration function $\chi = (2\pi/\lambda)\, W$. An illustration of the an ideal wave front and an aberration function is shown in figure 2.3

One common way to quantify and interpret the aberration function is to expand χ in some series where each of the basis corresponds to a specific aberration. One such aberration is the spherical aberration which originates from the use of spherical lenses. It deforms the beam such that rays that are far from the optical axis are mapped to a focus closer to the lens than those that propagate near the optical axis. The effect of spherical aberration is symmetric around $\hat{z}$.

Expressed in some cylindrical coordinates around the optical axis, χ is in optics often expanded into the orthogonal L^2 basis called the Zernike polynomials which are defined on the unit disc. The coefficients in a Zernike expansion are each associated with a specific type of aberration. Thus by projecting phase data on the Zernike polynomials it is possible to quantify the level of defocus, astigmatism, coma etc. in the beam. Using the far field equations in optics one may further on invert the wave propagation to understand the lenses.

Moving on, we would also be interested in the resulting image in the Gaussian focal plane given a wave aberration function χ. We define the image aberration δ as the two dimensional vector field in the Gaussian plane measuring the displacements of our aberrated beams from the ideal beam. The relation between wave and image aberrations is

$$\delta(x,y) = \frac{M\lambda}{\pi}\nabla\chi(x,y) \tag{2.6}$$

with M the magnification of the optical system. Using the above relation we can avoid the problem of measuring phase, instead comparing images to quantify aberrations.

2.2.2 In Electron Optics

In electron optics, aberrations are not as easily quantified nor are they as descriptive of the device the electrons have travelled through as in regular optics. To start with, perfect focusing as in Gaussian optics is impossible, even in theory. It was proven by Scherzer [2] that spherical and chromatic aberrations cannot be avoided if the following conditions are true simultaneously [12]:

1. The lenses are rotationally symmetric.

2. There is no charge on the optical axis.

3. The fields are static.

4. The optics produce a real image.

In order to eliminate these aberrations we must break at least one of the above conditions. In this work we have chosen to break symmetry because the technological outlook for this strategy seems the most promising. Space charge effects will sometimes be taken into account thus unintentionally and without benefit for beam quality, putting charge on the optical axis. Producing time varying fields, although possible, will not be considered due to the massive computational resources required. Also the last constraint must be kept if we want to focus our beam at all.

Problematic as it is, we must still define some ideal beam in order to measure aberrations. The canonical choice would be the same spherical wave found in perfect focusing conditions. A common way to express the wave aberration function in electron optics is

$$\chi(\theta,\phi) = \frac{\theta^{N+1}}{N+1}\Big(C_{NSa}\cos(S\phi) + C_{NSb}\sin(S\phi)\Big) \tag{2.7}$$

with θ inclination and ϕ azimuth in spherical coordinates [12]. We immediately notice the lack of L^2-orthogonality in the radial terms. Since it is only a Taylor series there is no guarantee for the convergence of the series when adding more terms. For the convergence to be possible we must not cross any singularities of the underlying function we are trying to fit [13]. Together with the degree of uncertainty in the sampled data [12] this forces us to put some effort in to choosing the power that we fit to. In practice the wave aberration function can be difficult to find and manufacturers of adaptive electron optics have chosen to measure the image aberration $\delta(x,y)$ instead. In the image plane we may then express a basis with the same coefficients as for the wave aberrations by simply differentiating the basis. The θ-component of the gradient is then

$$\frac{1}{r}\theta^N\Big(C_{NSa}\cos(S\phi)+C_{NSb}\sin(S\phi)\Big) \tag{2.8}$$

and the ϕ-component is

$$\frac{S}{r\sin\theta}\frac{\theta^{N+1}}{N+1}\Big(-C_{NSa}\sin(S\phi)+C_{NSb}\cos(S\phi)\Big). \tag{2.9}$$

Setting r to constant leavs only two dimensions.A choice of basis has been made with a close relation ideal magnetic multipole fields. The scalar potential of such a field with $2N$ poles is expressed as

$$\Phi(\rho,\phi)=\rho^N\Big(p_N\cos(N\phi)+q_N\sin(N\phi)\Big) \tag{2.10}$$

with ρ radius and ϕ azimuth in cylindrical coordinates. We will explore the uses of these fields further in section 2.3.

Note that one can also choose to represent the two dimensional euclidean space in the complex plane. Let the complex variable

$$\omega = x + iy \tag{2.11}$$

represent our position vectors with $\bar{\cdot}$ denoting complex conjugation. Then we have the complex wave aberration function

$$W(\omega,\bar{\omega})=\mathrm{Re}\sum_{N,M}c_{N,M}\omega^N\bar{\omega}^M. \tag{2.12}$$

Using some of the multiplication properties of complex numbers we note that the power is $p = N + M$ and the symmetry $s = |N - M|$. We further add implicit rules for N and M to get uniqueness for our representation. This is done by requiring $p \geq s$ and that p and s share the same parity. With these rules we find ourselves with the basis described in table 2.1 and visualized in figure 2.4.

The gradient in Euclidean space is equivalent to

$$2\frac{\partial W}{\partial\bar{\omega}} \tag{2.13}$$

in the complex plane [14]. Using this formulation the gradient lies in the complex plane as well, making calculations such as least squares fitting rather convenient.

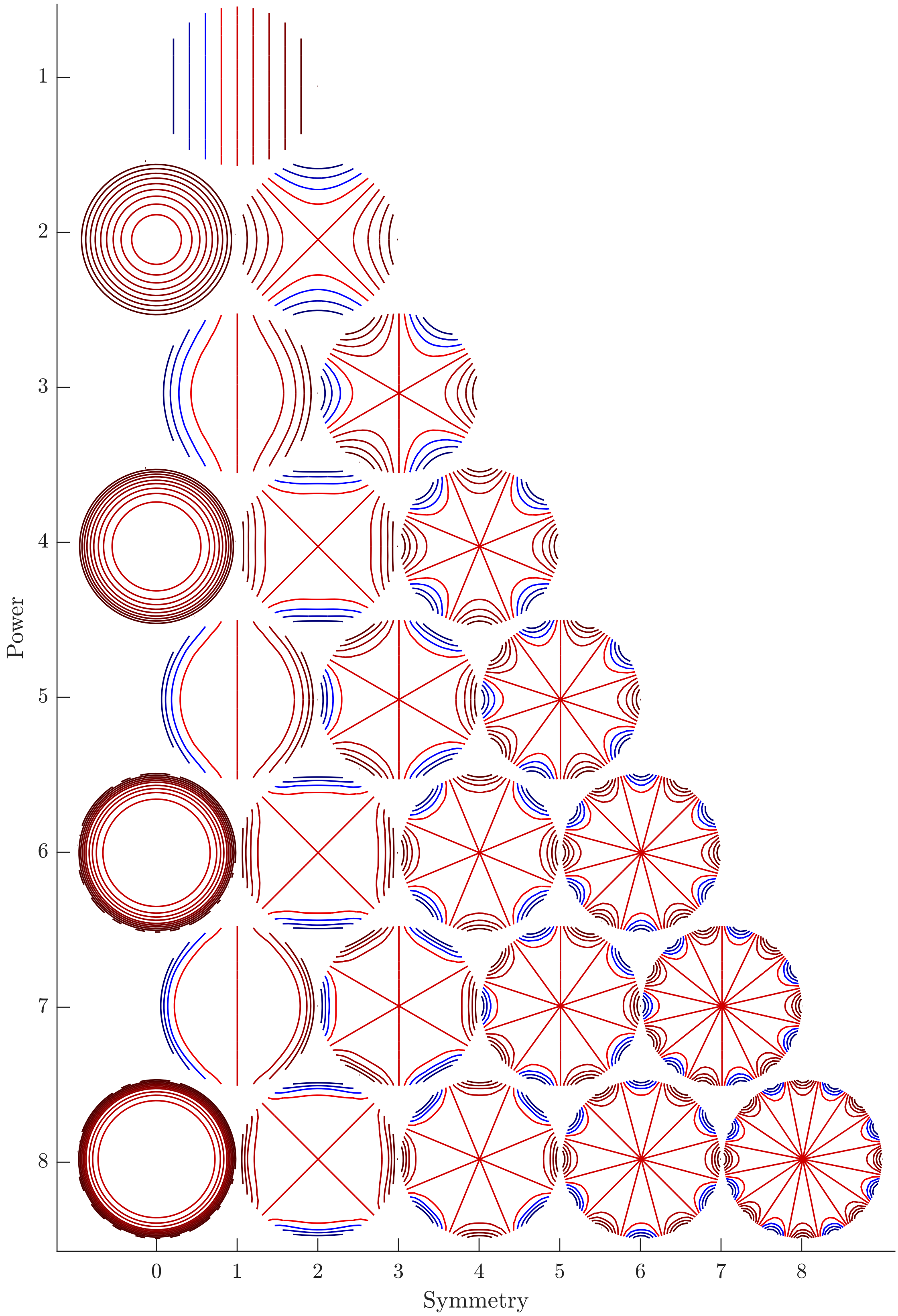

Figure 2.4: Contours of the first 24 cosine wave aberration functions or real part of the complex wave aberration functions named in table 2.1. The blue denotes negative unity while dark red represents positive one. Note that the remaining bases needed for completeness on the unit disc are only half period rotations of the above.

Table 2.1: Complex wave aberration basis functions with names from [14]. The first 24 functions are written here and also illustrated in figure 2.4. Note that the basis is not normalized here.

Index	Name	Power	Symmetry	Expression
1	Shift	1	1	$\bar{\omega}$
2	Defocus	2	0	$\omega\bar{\omega}$
3	Twofold astigmatism	2	2	$\bar{\omega}^2$
4	Second-order axial coma	3	1	$\omega^2\bar{\omega}$
5	Threefold astigmatism	3	3	$\bar{\omega}^3$
6	Third-order spherical aberration	4	0	$\omega\bar{\omega}^2$
7	Third-order star-aberration	4	2	$\omega^3\bar{\omega}$
8	Fourfold astigmatism	4	4	$\bar{\omega}^4$
9	Fourth-order axial coma	5	1	$\omega^3\bar{\omega}^2$
10	Fourth-order three-lobe aberration	5	3	$\omega^4\bar{\omega}$
11	Fivefold astigmatism	5	5	$\bar{\omega}^5$
12	Fifth-order spherical aberration	6	0	$\omega\bar{\omega}^3$
13	Fifth-order star-aberration	6	2	$\omega^4\bar{\omega}^2$
14	Fifth-order rosette aberration	6	4	$\omega^5\bar{\omega}$
15	Sixfold astigmatism	6	6	$\bar{\omega}^6$
16	Sixth-order axial coma	7	1	$\omega^4\bar{\omega}^3$
17	Sixth-order three-lobe aberration	7	3	$\omega^5\bar{\omega}^2$
18	Sixth-order pentacle aberration	7	5	$\omega^6\bar{\omega}$
19	Sevenfold astigmatism	7	7	$\bar{\omega}^7$
20	Seventh-order spherical aberration	8	0	$\omega\bar{\omega}^4$
21	Seventh-order star-aberration	8	2	$\omega^5\bar{\omega}^3$
22	Seventh-order rosette aberration	8	4	$\omega^6\bar{\omega}^2$
23	Seventh-order chaplet aberration	8	6	$\omega^7\bar{\omega}$
24	Eightfold astigmatism	8	8	$\bar{\omega}^8$

2.3 Magnetic Multipole Lenses

While in principle an arbitrarily shaped magnetic field could be used to manipulate the particle trajectories, only magnetic stigmator lenses have in been used in practice. Here we present the lowest order multipoles along with their applications.

2.3.1 Solenoid lens

The focusing solenoid lens is a fundamental component in electron optics. By aligning its field with the optical axis it causes the electrons to curve in a circular motion towards the optical axis. The reciprocal z-coordinate for the disc of least confusion is then given by [9]

$$1/f = \frac{e^2}{8mE_0} \int B_z^2 \,\mathrm{d}z \tag{2.14}$$

with a rotation angle of

$$\phi = \frac{e}{\sqrt{8mE_0}} \int B_z \,\mathrm{d}z. \tag{2.15}$$

Further on one can gain some insight if the field is assumed to be Lorentzian or Cauchy distributed along the optical axis.

$$B_z = B_0 \frac{1}{1 + \frac{z^2}{a^2}}. \tag{2.16}$$

This results in a focusing power given by

$$1/f = \frac{\pi}{16} \frac{e^2}{mE_0} a B_0^2 \tag{2.17}$$

which for $f = 1\,\mathrm{m}$ and a coil height $a = 10\,\mathrm{cm}$ requires $B_0 = 4\,\mu\mathrm{T}$.

2.3.2 Orthogonal Dipole

A coil that induces a magnetic field orthogonally to the optical axis will function as a beam deflector. From the Lorentz force equation it is clear that the magnetic will deflect the beam in the direction that is orthogonal to both the magnetic field and the optical axis. Commonly the fields of two independently controlled dipole pairs are superposed to form a deflection with an arbitrary orientation.

If the deflection field is completely homogeneous and the incoming electrons travel along the optical axis, the deflection will eventually make the electrons move in a circle with radius [15]

$$r = \frac{mv_0}{eB_0}. \tag{2.18}$$

This can be seen from solving the classical equations of motion for an electron in a homogeneous magnetic field $\mathbf{B} = B_0\hat{x}$

$$m\dot{v}_y(t) = B_0 q v_z(t) \tag{2.19}$$

$$m\dot{v}_z(t) = -B_0 q v_y(t) \tag{2.20}$$

Differentiating once with respect to time and substituting the velocities we obtain a homogeneous Helmholtz equation. With the initial conditions

$$v_y(0) = 0 \tag{2.21}$$
$$\dot{v}_y(0) = \tfrac{B_0 q}{m} v_0 \tag{2.22}$$
$$v_z(0) = v_0 \tag{2.23}$$
$$\dot{v}_z(0) = 0 \tag{2.24}$$

we obtain the solution

$$v_y(t) = v_0 \sin\left(\tfrac{qB_0}{m} t\right) \tag{2.25}$$
$$v_z(t) = v_0 \cos\left(\tfrac{qB_0}{m} t\right). \tag{2.26}$$

The deflection angle is then simply

$$\alpha = \arctan \frac{v_y}{v_z} = \frac{qB_0}{m} t. \tag{2.27}$$

Now assuming that the field is zero for $z > a$ such that $B_0 q/m \gg t_a$ we may substitute $t = z/v_0$ to approximate the angle with

$$\alpha = \frac{B_0 q}{m} \frac{a}{v_0}. \tag{2.28}$$

As an example a 60 keV electron in a field that is 10 cm long and 1 mT strong will be deflected 120 mrad.

2.3.3 Quadrupole

The coils used for generating dipole fields are aligned such that the direction of the fields of two opposing poles have the same direction across the optical axis. Quadrupole fields, on the other hand, are generated by orienting opposing dipole fields on opposite sides of the optical axis. This means that the fields have to bend outwards and vanish at the center in order for the divergence theorem to hold. The effect on a charged particle beam is then focusing along one axis and defocusing along the other, as illustrated in figure (2.2b). Consequently a correctly aligned quadrupole stigmator may be used to shape an elliptical beam to a circular one, thus correcting two-fold astigmatism.

2.3.4 Hexapole

In the hexapole[1] stigmator the fields alternate from pointing inward to pointing outward three times. Hexapole stigmators are through their threefold symmetry able to remove threefold astigmatism.

[1] All other multipoles are enumerated using the Latin prefix which means that the correct name would be Sextupole. However, we have chosen to use the far more common Greek enumeration for stigmators with six or sixteen poles.

Hexapoles are used in more sophisticated arrangements to remove spherical aberration in electron microscopes. In such a corrector two hexapoles are positioned one after the other. The first one mitigates third order spherical aberration but introduces three-fold astigmatism. The second one is rotated one third of a revolution such that the three-fold astigmatism is nullified. What remains after is a beam that has only been affected by the radial effects which happen to reduce spherical aberration.

2.3.5 Octupole

Octupole stigmators also consist of fields alternating their radial direction. The symmetry here is fourfold which in principle enables us to correct four-symmetric aberrations.

Another way of using octupoles is in a quadrupole-octupole spherical aberration corrector. In such a correction device four quadrupoles and three octupoles are interleaved symmetrically. Once again the technique of inverting the symmetries in the highest order multipoles is used. Here the first and the third octupoles introduce four-fold astigmatism as they remove spherical aberrations in the x and y directions respectively. The octupole in the middle corrects four-fold astigmatism.

2.4 The Finite Element Method

The finite element method (FEM) is a method for finding approximative solutions to Partial Differential Equations (PDE). In FEM the solutions are projected on a finite space of known functions. Also the PDE is reformulated in the weak sense, such that solutions only need to converge in inner product with test functions. This will results in the solution having a scalar error which can be optimized using known methods. The resulting optimization problem almost always includes working with high dimensional sparse matrices. The larger class of methods that involve taking the inner product of a problem with test functions and optimizing are also known as variational methods.

2.4.1 Finite Element

A *finite element* is defined in [16] as a triple (T, V, L) such that

- the domain T is a closed and bounded subset of $\mathbb{R}^N$ with nonempty interior and piecewise smooth boundary.
- the space $V = V(T)$ is an n dimensional function space on T.
- the degrees of freedom $L = l_1, l_2, ...l_n$ form a basis for the space of linear bounded functionals on V.

The textbook example of a finite element is the linear Lagrange element in one dimension which can readily be used for solving scalar PDEs. Here T is simply a line, V is the space of first degree polynomials on T and is point evaluation on the vertices [16]. T is commonly referred to as the *mesh* element.

2.4.2 Variational Formulation of Magnetostatics

The problem at hand is accurately described by Maxwell's equations in their differential forms. We are looking for the magnetic field $\mathbf{H}$ with flux density $\mathbf{B} = \mu\mathbf{H}$ defined on $\Omega \subseteq \mathbb{R}^3$ given a charge carrying current density $\mathbf{J}$ defined on that same set, that fulfill

$$\nabla \times \mathbf{H} = \mathbf{J} \tag{2.29}$$

$$\nabla \cdot \mathbf{B} = 0. \tag{2.30}$$

On the boundary $\partial\Omega$ with normal vector $\mathbf{n}$ we do not allow $\mathbf{B}$ to point outward. In other words

$$\mathbf{B} \cdot \mathbf{n} = 0. \tag{2.31}$$

The above boundary condition is called perfect magnetic insulation. In practice it could be realized through the use of insulators called Mu-metals with relative permeabilities of 100 000 [17]. A variational form suitable for FEM which will be used here is

$$F(\mathbf{A}) = \frac{1}{2}\int_\Omega \frac{1}{\mu_r}(\nabla \times \mathbf{A}) \cdot (\nabla \times \mathbf{A}) - \mu_0 \mathbf{A} \cdot \mathbf{J}\,\mathrm{d}\mathbf{r}. \tag{2.32}$$

It can be proven that when the functional F is stationary with respect to $\mathbf{A}$ equations 2.29 and 2.30 are fulfilled [18].

2.4.3 Discretization Using Vector Elements

In order to optimize equation 2.32 on a numerically we will discretize $\mathbf{A}$ by projecting it on to some finite function space defined on some subset of $\mathbb{R}^3$. Using the Lagrange elements would in this case not enforce the divergence condition thus resulting in so called spurious or unphysical solutions. Penalty methods have previously been used to avoid this but were only successful in systems with low contrast in μ [18]. Since magnetic polepieces often have μ_r on the order of 10^4 and are necessary for strong focusing the penalty method cannot be used here.

Instead we shall use the rather modern notion of vector or edge elements. In 1980 J.C. Nedelec published an article [19] on tetrahedal and cubic elements. These elements were equipped with the function spaces $H(\mathrm{curl})$ and $H(\mathrm{div})$ having curls and divergences respectively that are L^2 integrable on their elements. What is special about the so called Nedelec elements elements is that the degrees of freedom are not nodes but vectors [18].

2.5 Charged Particle Tracing

Once the magnetic fields induced by the lenses have been solved for, the next step is to compute the resulting force acting on the moving electrons. The problem is well known and has formal solutions ranging in computational complexity from none to impossible. One could for example attempt to solve the Schrödinger equation with the magnetic potential from the lenses and electric and magnetic potential from some billion particles. Special relativity is yet another part of physics that is part of the problem. Clearly, we must make some assumptions and approximations. In this section we will describe the physical effects that have been taken into account and afterwards motivate the lack of others.

2.5.1 Lorentz Force and Classical Physics

Moving charge interacts with magnetic fields. In classical physics the Lorentz force and the gravitational force together with Newton's equations of motion fully cover the dynamics of electrons. We will later see that the acceleration of free falling massive bodies of $9.8\,\mathrm{m/s^2}$ is completely negligible compared to the acceleration from the Lorentz force in our problems. Therefore, we chose to not include gravity in the model and only take the Lorentz force 2.1 into account.

2.5.2 Magnetic Fields from Lenses

To give a sense of scale the resulting acceleration for an electron with a kinetic energy of $60\,\mathrm{keV}$ in a magnetic field of $100\,\mu\mathrm{T}$ is on the order of $10^{15}\,\mathrm{m/s^2}$. Such an electron travels at almost half the speed of light. Clearly the effect of magnetic fields will dominate the dynamics of the system.

2.5.3 Space Charge

The second term in equation 2.1 could originate from electrostatic lenses and the electrons themselves. In this thesis we will not study systems that utilize electrostatic lenses. Therefore we shall only investigate the effect of the electric fields from the electrons in the beam, known as space charge. The electric field of a distribution of N point charges in vacuum at positions $\mathbf{r}_i$ with charge q is

$$\mathbf{E}(\mathbf{r}) = \sum_i^N \frac{q}{4\pi\epsilon_0} \frac{\mathbf{r} - \mathbf{r_i}}{|\mathbf{r} - \mathbf{r_i}|^3}. \tag{2.33}$$

The resulting forces in the beam will then require the calculation of N contributions for each particle resulting in a quadratic computational complexity. Having enough particles for exactly simulating a current of some $10\,\mathrm{mA}$ is consequently problematic since this corresponds to an electron density of $10^{10}\,\mathrm{cm^{-3}}$ at $60\,\mathrm{keV}$.

A solution for this problem is to simulate fewer particles but with a so called charge multiplication factor p. For this reduced model we only simulate N/p particles for N physical particles.

To simplify even further the distance calculations can be reduced by binning the charges to domains in space and using the centroid of the domain and the sum of the charges inside as a point source for the E-field. Normalizing to domain volume we call the piecewise constant quantity

$$\rho_i = \frac{\int_{\Omega_i} \sum_j^{N/p} p\delta(\mathbf{r}_j)\,\mathrm{d}\mathbf{r}}{\int_{\Omega_i} \mathrm{d}\mathbf{r}} \tag{2.34}$$

the space charge density. Here Ω_i denotes the binning domain and $\mathbf{r}_j$ the positions of the M charged particles that are actually in the simulation. Recasting ρ_i to a function on a continuous domain we obtain

$$\rho_s(\mathbf{r}) = \rho_i,\ \mathbf{r} \in \Omega_i. \tag{2.35}$$

2.5.4 Special Relativity

Using Einsteins mass energy relation

$$E = mc^2 = m_0\gamma(v)c^2 \tag{2.36}$$

where m_0 is the rest mass of a particle and v its velocity, we know that electrons with a kinetic energy of 60 keV move at a velocity of $0.45c$. For this velocity we have $\gamma = 1.2$ which warrants use of special relativistic equations of motion instead of the Newton ones.

$$\mathbf{F} = \frac{\mathrm{d}}{\mathrm{d}t}\Big(m_0\gamma(v)\mathbf{v}\Big) \tag{2.37}$$

For analytical calculations the nonlinearity in v is devastating. For such calculations the Lagrangian formulation is probably more suitable, but here we will mostly focus on numerical solutions which is why the equations of motion above are satisfactory.

2.5.5 Putting it all together

The resulting equation of motion for the effects described above is

$$\frac{\mathrm{d}}{\mathrm{d}t}\Big(m_0\gamma(v)\mathbf{v}\Big) = q\Big(\mathbf{v}\times\mathbf{B} + \mathbf{E}\Big) \tag{2.38}$$

with $\mathbf{B}$ from the magnetic lenses and $\mathbf{E}$ from the space charge density. Finally we could also note that we could simplify our problem by expanding γ to zeroth order around the mean initial velocity. This is motivated by the inability of the magnetic fields to exert work on the particles which implies that their velocities should be close to constant during the short time simulated.

2.5.6 Effects not included in the model

One effect not included in the model is the force resulting from B fields from the moving electrons. The field from N charges at positions $\mathbf{r}_i$ and velocities $\mathbf{v}_i$ evaluated at $\mathbf{r}$ is given by

$$\mathbf{B}(\mathbf{r}) = \sum_i^N \frac{\mu_0 q}{4\pi}\mathbf{v_i}\times\frac{\mathbf{r}-\mathbf{r}_i}{|\mathbf{r}-\mathbf{r}_i|^3}. \tag{2.39}$$

The resulting force on the electrons thus scales as Nv^2/r^2 which might sound alarming for a fast dense beam. Now we may note that the Lorentz force from this field will have a factor of $\mathbf{v}\times\mathbf{v}_i$ in it with $\mathbf{v}$ the velocity of the electron for which we are calculating the force. This means that we may safely neglect it if the velocities of the particles are in the same direction. In other words, we have to assume that our beam emittance is close to zero.

Further, in this thesis we will not take the quantum wave nature of electrons into account. This is motivated by difference in scale between what we investigate and the de Broglie wavelength of the electrons. For 60 keV electrons we have $\lambda = 2\,\mathrm{pm}$ while our smallest aperture is some ten centimeters. Therefore we may safely assume that diffraction will not be seen in our simulations even if properly modelled.

We shall avoid modeling vacuum imperfections or parasitic electromagnetic fields such as the magnetic field of the earth. However, the modeling framework is well suited to model the impact of these non-ideal conditions in future studies.

Chapter 3

Methods

The majority of the project has been dedicated to developing methods for accurately simulating magnetic fields and charged particle trajectories as well as tools for interpreting the results. In this chapter we begin by presenting the general methods used with COMSOL Multiphysics® in the first section. Then we move on to an overview of the final coil model in section 3.2 with a history of its predecessors. Finally section 3.3 details how the postprocessing of the simulation data was done.

3.1 Modeling magnetic fields and charged particle tracing in COMSOL Multiphysics

Both the magnetic fields and the trajectories of the electrons need to be modeled when analyzing the aberrations of an electron optical system. COMSOL solves the magnetic fields and self-consistent particle trajectories using a finite element method. This section will detail how a model for the magnetic fields and particle trajectories is realized using COMSOL as well as how the model is used to generate data for the study of the system aberrations.

The COMSOL model can be divided into groups of active and passive components. The active components are sources such as the coil lenses and the surface inlet where the electron beam is initiated. The passive components are not directly contributing to the magnetic field or the electron trajectories but rather provide the material properties and boundary conditions in the model. Examples of passive components are the toroidal cores around the coils, the perfect vacuum and the outer boundaries of the model.

3.1.1 COMSOL model overview

The model is defined inside the vacuum cylinder which limits the extent of both the magnetic fields and the particle trajectories. The cylinder is 1 m high and has a radius of 10 cm which matches scales commonly used in EBM systems. The boundaries of the cylinder are modeled as perfect magnetic insulators which means that there is no magnetic fields in the direction normal to the surface of the boundary.

The electrons are initialized at the center of the bottom of the vacuum cylinder with a velocity corresponding to a kinetic energy of 60 keV in the positive z-direction.

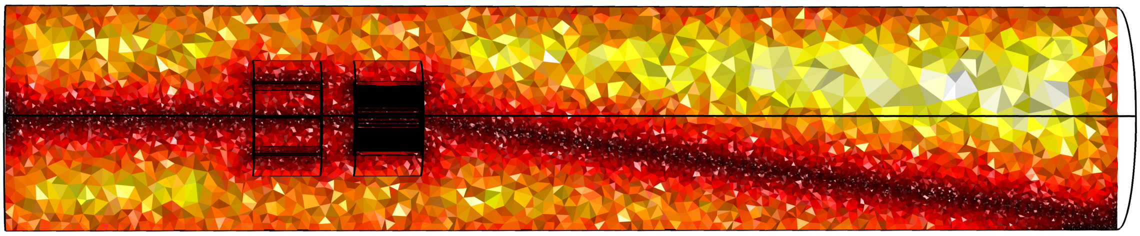

Figure 3.1: Cut through of the mesh used in the COMSOL model where the color corresponds to the size of the mesh elements. Electrons travel from left to right. Note how the fine mesh structure follows the expected beam path after the deflection coil.

The electrons then pass through the magnetic lenses which focus, deflect and correct the electron beam. A detailed account of how the magnetic lenses are modeled is given in the following section. The electrons continue past the magnetic lenses and towards the top of the vacuum cylinder. Space charge repulsion is the dominating force on the electrons in this region since the magnitude of the magnetic field decreases as the electrons move away from the magnetic coils.

3.1.2 Meshing in a Finite Element Method Model

While the model's geometry is defined parametrically the model needs to be discretized before it can be solved using the finite element method. The discretizantion involves dividing the geometry of the model into 3-dimensional shapes, the so-called finite elements, which are collectively called the mesh. These elements are irregular tetrahedrons which fill the entire volume of the model. The choice of how to divide the model geometry is non-trivial and impacts both the performance and accuracy of the solver. Most implementations are based on a trade-off between having many small elements with a high accuracy and fewer and larger elements which results in a smaller numerical problem.

3.1.3 Meshing in the COMSOL Model

The meshing in COMSOL Mutiphysics® is performed using a semi-automatic meshing algorithm which divides the geometry based on several factors. One of the main goals of the optimization is to maximize the mesh element quality which refers to the shape of a specific mesh element. The mesh element quality is a measurement of how close the mesh element is to being an regular tetrahedron which means that the algorithm will try to avoid elongated elements.

It is possible to only use the automatic meshing function in COMSOL without any tuning and get satisfactory results. However, this may not be the case when modeling charged particle tracing and magnetostatic fields at the same time. This is due to the large difference in the precision requirement between the magnetic lenses and the size of the electron beam. This problem is even more prominent since the models include a space charge effect between the electrons. The meshing process is therefore modified such that the size of the mesh elements is much smaller in the regions where the electron beam is expected to be, as shown in figure 3.1. This will minimize the error in the beam trajectory modeling without needlessly increasing the number of mesh elements in volumes significantly far away from the beam.

3.2 Modeling magnetic coil lenses

The following section will detail how compounded multipole coils can be modeled using the finite element based software COMSOL Multiphysics. The task of modeling complex coils is not trivial and requires a trade-off between the reliability of the results and the complexity of the models. There is also a need for the model to be flexible enough to allow the user to alter the parameters of the coil without having to rebuild the entire model.

One of the problems in modeling an electron optical system is formulating an accurate description of the coils that constitute the magnetic lenses. On one hand, there is a need to include as much detail as possible in the coil-models in order to capture the effects of geometrical asymmetries and perturbations on the electrons' trajectories. On the other hand, the finite element method used to compute the magnetic fields and electron trajectories imposes limits on the geometric complexity of the models. These limits result from the fact that the number of elements, and therefore number of degrees of freedom, increase with the geometric complexity which in turn increase both the memory requirement and the time needed to solve the model.

Separate considerations also need to be taken in relation to how the currents in the coils are modeled. In an ideal model each wire in the coil would be modeled separately, both in terms of geometry and current. This is not feasible when the scale of a single wire is significantly smaller than the surrounding geometry. COMSOL Multiphysics circumvents this by modeling the wires in a multi-turn coil by defining a vector-field describing the current directions in a geometric domain.

For instance, a solenoid coil is modeled in a hollow cylinder with the current vector-field defined as the angular component in a cylindrical coordinate system. A more complicated coil, such as the deflection coils that are composed of several compounded dipoles coils, needs a more precise description in order to capture the detailed magnetic fields of the coil.

3.2.1 Models of deflection and aberration coils

There are three functions that the coils need to perform: focusing, deflection and aberration correction. The focus coil is comparatively easy to model since it is a simple solenoid wound on a cylinder. The aberration and deflection coils on the other hand need a more detailed model since the behavior of the magnetic fields, and therefore the electron beam, is the result of the interaction between several independent coils that are not wound in a rotationally invariant configuration. While the basic function of these coils can be modeled using simplified models, many of the details can not be removed without altering features in the magnetic field. Careful consideration needs to be taken regarding which features that can be omitted since many of the aberrations arise from a non-ideal magnetic field.

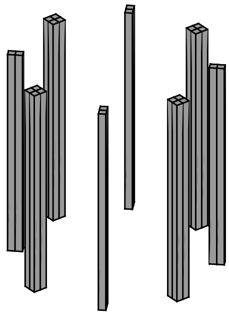

(a)

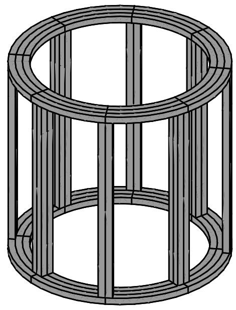

(b)

Figure 3.2: Renders of the bar-model **(a)** and closed circuit-model **(b)** used to simulate a quadrupole coil.

Both the aberration and deflection coils works by generating magnetic fields that are perpendicular to the optical axis of the lens system and beam-line. One of the main goals when designing these coils is to induce a magnetic field that is as homogeneous as possible while still being able to steer the beam in a sufficiently short amount of time. This is achieved by winding the individual poles on a sinusoidal distribution on the surface of a cylinder. Such a coil will result in a homogeneous magnetic field at the center of the coil. Each of the individual poles spans half the circumference of the cylinder and therefore overlaps with the neighboring poles. The deflection coils are composed of 4 such poles placed at a relative angle of 90° in order to allow full control of the beam deflection. An angle of 45° or 135° between the poles in the aberration coils is required for full angular control of the aberration correction. Both of these designs are based on winding several individual coils on the same coil core which results in a complexly wound coil. Much of the work of this project has been devoted to describing both the geometry and directional vector fields of the currents in terms that are usable to a finite element solver.

Bar model

One very simple way of modeling the aberration and deflection coils is based on omitting the horizontal parts of the coils leaving only vertical "bars". These bars would be arranged in pairs along a cylindrical shape where each pair represents a circle in the coil as illustrated in figure 3.2a. The current direction in each bar would be either along or against the beam direction which can easily be modeled in COMSOL. The resulting geometry is simple to model given that the bars are sufficiently thick. A very thin bar would require very small elements both in the bars and their surroundings which may result in a model with too many elements for us to able to solve our hardware. The two major drawbacks of this approach is the omission of horizontal currents at the top and bottom of the coil and the number of bars required in order to construct a higher order[1] coil. The omission of

[1] Higher order in this context means a higher number of poles in the coil.

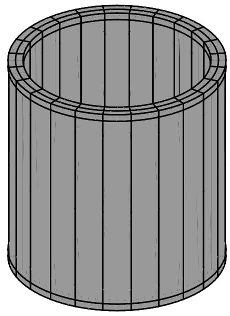

Figure 3.3: Render of a coil based on the superposition model divided into 24 angular segments.

the horizontal parts of the coil affects how the magnetic fields propagate outside of the coil along the optical axis.

Closed circuit model

The lack of horizontal components in the bar model and the associated error lead to the closed circle model where an arc of a circle was added to the top and bottom of a pair of bar as shown in figure 3.2b. The resulting geometry creates a closed circuit where the currents are directed around a horizontal rotational axis. While the closed circuit geometry is simple it does not allow the user to change the pole configuration of the coil without significantly altering the model. Also, the number of layers needed will increase linearly with the number of poles since a bar or arc can only contain a single current field. This means that the error from placing the poles at different radii will increase with the number of poles in the coil.

The currents in the closed circuit model can be easily described by a vector field defined on the four domains of the modelled pole. The vector field is simply positive or negative in the z-direction or along or against the angular component in a cylindrical coordinate system.

3.2.2 Superposition model

The problem of creating a model that manages to accurately represent the desired physical properties as well as being flexible enough to allow parametric studies of the electron optical system occupied a large part of this project. This is achieved by modeling a coil consisting of a superposition of many coils that represent many poles. The sum of the current fields from all poles is computed and placed in two cylindrical shells. The rationale for dividing the coil in two shells with opposing current directions is that two currents with opposite directions do not cancel each other. However, calculating the resulting current density vector field is practically impossible to implement in COMSOL without the ability to automate the generation of the superposition coil.

The superposition model is in principle very similar to the closed circuit model where each closed loop in the coil is modeled by six segments: two bar segments and four arc segments. One of the main differences is how the geometry of the coils are modeled. The geometry of the superposition model is simply a hollow cylinder composed of two layers that are divided in a suitable number[2] of times along the optical axis. The thinness of the two shells is limited by the number elements that can be included in the FEM solver. Each angular segment is finally divided along the optical axis into three parts: the bottom arc segment, the bar segment and the top arc segment as shown in figure 3.3. This means that the total number of segments for the entire coil is equal to six times the number so angular segments which is why it would be impractical and time consuming to define all of the coil objects using the COMSOL GUI. A faster and more flexible method is to use the scripting capabilities enabled by linking COMSOL to MATLAB.

The direction of the current is defined in a similar way as the closed circuit model where the vector field is parallel to the optical axis or the angular basis vector in a cylindrical coordinate system. The two cylindrical layers are used to separate the two possible directions of the vector field in each segment pair. Specifically; the direction of the inner bar segments is reserved for currents directed downward and the inner bar segment for the upward directed currents. The clockwise and counterclockwise currents are divided between the inner and outer top and bottom arc segments in a similar way. This will be the source of a modeling error since the two cylindrical shells have a non-zero thickness and different parts of the same coil will be at radii from the optical axis.

The superposition model is, as the name suggests, based on superposing several independent poles and into a single configuration of currents directions and magnitudes. The basic building block for the superposition is a multipole wound on the shell of a cylinder. The angular width along the shell of a single pole is $4\pi/n$ where n is the order[3] of the superposed coil. This means that there will be an overlap of two single poles at any given angle along the cylinder. The numbers of turns in the single pole varies in a sinusoidal pattern along the shell of the cylinder, reaching a maximum at the center of the pole.

The superposition is computed by adding the current contribution from each of the individual poles in every segment of the superposed coil. For instance, in a superposed coil with 24 angular segments there are $6 \times 24 = 144$ segments that are assigned a calculated current. Since updating all 144 currents manually using the COMSOL GUI would be both time consuming and error prone, LiveLink[4] for MATLAB[5] is used to update the currents in the model. By using this method both the computation and input of the currents can be performed without altering the geometry of the COMSOL model. This is not only time saving but allows the user to only alter the functionality of the coil while keeping the rest of the model static, allowing for easy comparisons.

All of the results in this report are produced using the superposition model given

[2] A number with high divisibility such as 12, 24 and 48 are particularly useful

[3] The number of dipoles in the configuration, e.g $n = 4$ for a quadrupole

[4] LiveLink is a registered trademark of COMSOL AB

[5] MATLAB is a registered trademark of The MathWorks, Inc.

its simplicity and flexibly. A model with many poles, such as 16 or 24, would have introduced large errors in the min bar- and closed circuit-models due to the difference in radii of the poles. A possible solution to this would have been to decrease the thickness of each layer. This would, however, greatly increase the both the memory requirement and solution time of the model.

3.3 Data analysis

In this section we present the methods for finding aberration functions from particle positions given by COMSOL.

3.3.1 Finding the Plane of Least Confusion

Finding the aberrated equivalent to a focal point was done in the post processing step in MATLAB. The particle phase space data was exported from COMSOL at all time steps that were solved for. In MATLAB linear interpolation was used to trace the particles between the time steps of the solution. Further a routine for making Poincaré sections was made so that the images at different distances along the optical axis could be viewed. On these sections we could then evaluate measures of confusion and then run one of MATLAB's optimization tools to find the plane of least confusion.

The measure selected was the variance of the particle x and y positions in the section. Other measures were also investigated, such as the full width at half maximum and the number of particles within a circle with small radius. The variance method proved to be the most general and robust measure. The drawback of only looking at variance is that detail is lost and that there is little intuition for beams with non-normally distributed particle positions such as hollow beams.

3.3.2 Finding the Aberration Coefficients

To measure our aberration coefficients information about the wave aberration function is needed. Since measuring the phase of a beam directly is difficult a more practical approach, similar to the one used by Krivanek et Al [20], was chosen.

First we simulated a reference beam, that was only focused without any deflection or aberration correction. This beam took the place of the Gaussian beam in optics and all aberrations were measured using it as a reference. Its plane of least confusion was found and a Poincaré section made through it. The initial phase space conditions of the reference beam were used again for a system with the same focus settings but also with deflection. Also for this beam a Poincaré section was made at the focal point of the reference beam. Since the particles were the same as for the reference beam finding samples of the image aberration function simply became a matter of subtracting the particle positions.

These samples were then fit to the gradient of the truncated series of the wave aberration function with MATLAB's backslash routine. Since the coefficients in the gradient are the very coefficients of the Wave Aberration Function the aberration spectrum was then extracted.

3.4 Correcting Aberrations

The correction step was done manually. The image was inspected and its shape was used to select a trial domain for the corrector settings. The simulations were then made with a coarse grid of settings in the trial domain. The inspection and domain selection process was then repeated with a finer grid on a smaller domain. This approach has its limitations and was only used for Quadrupole and Hexapole correctors. That meant varying only the magnitudes and orientations of two fields.

For higher order, or finer correction optimization algorithms were considered but deemed hard to use due to each simulation being about 20 minutes long.

Chapter 4

Results

In order to verify the methods presented in the previous chapter ample data needed to be collected and processed. In this chapter we present results for magnetic fields with up to 24 poles as well as properties of simulated beams.

4.1 Magnetic Fields

The first half of the solver sequence is used for computing the magnetic fields that are generated by the coil lenses. These results are then used to model how the electron trajectories are effected by the Lorentz force. Some results form the the magnetic field model are shown in this section.

4.1.1 Focus lens

The magnetic focus lens needs to be the strongest source of magnetic field in the model in order to focus the electron beam. A plot of the magnetic field magnitude and direction in the center plane of the lens is shown in figure 4.1. The distribution of the fields on the z-axis is shown in figure 4.2.

4.1.2 Deflection lens

The deflection lens works by inducing a magnetic field perpendicular to the optical axis using a multipole coil. The poles are used to steer the direction of the magnetic field and by extension the electron beam. Two configurations of a multipole coil used as a deflection lens is shown in figure 4.3. Figure 4.3a shows a deflection lens where the deflection field is completely aligned with one of the pairs of poles in a quadrupole coil. A deflection coil where the deflection field is at an angle of $\pi/4\,\mathrm{rad}$ in relation to the pole axes is shown in figure 4.3b. The fields from these coils are shown on the z-axis in figures 4.4 and 4.5.

4.1.3 Stigmators

One of the major advantages of the superposition coil model is the fact that many different order stigmator coils can be modeled without altering the geometry of the

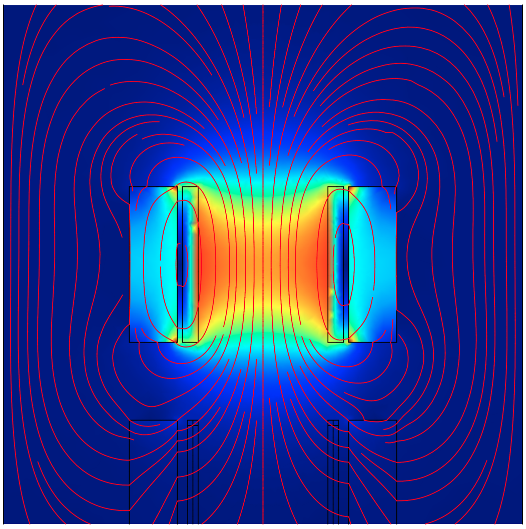

Figure 4.1: Plot of of the magnetic field induced by the focus coil in a plane parallel to the optical axis. The direction of the field is plotted as red streamlines and the magnitude as the colored background which is coded from blue to red.

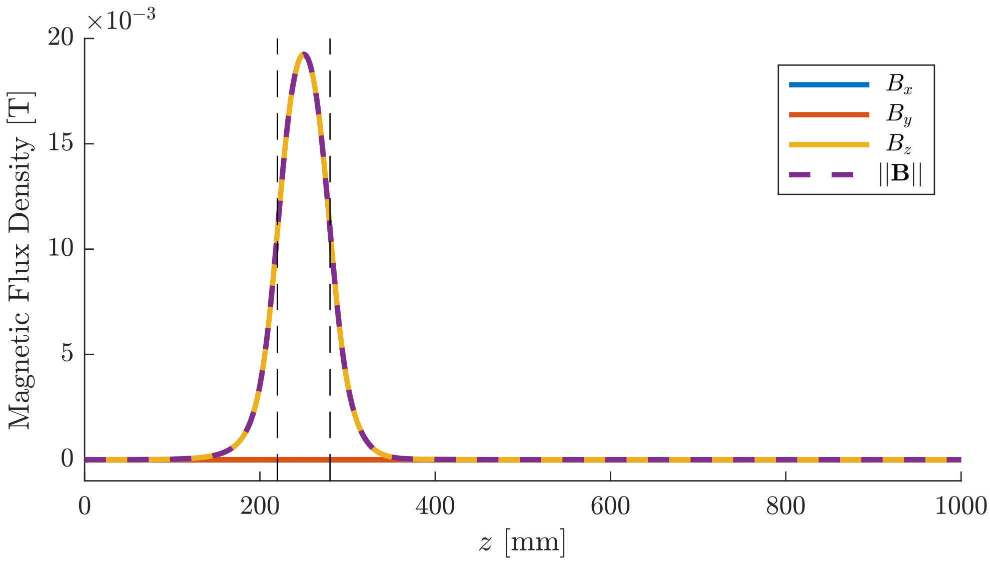

Figure 4.2: Magnetic fields on the z-axis from a focusing lens. The lens physically extends from the left dashed vertical line to the right.

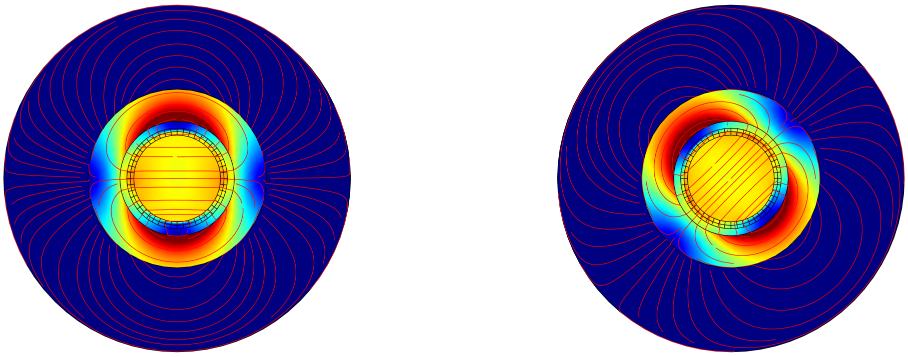

(a) **(b)**

Figure 4.3: Plot of the magnetic field from a deflection lens where the deflection field is **(a)** aligned with the pole axes and where the deflection field is **(b)** at a $\pi/4$ rad angle in relation to the pole axes.

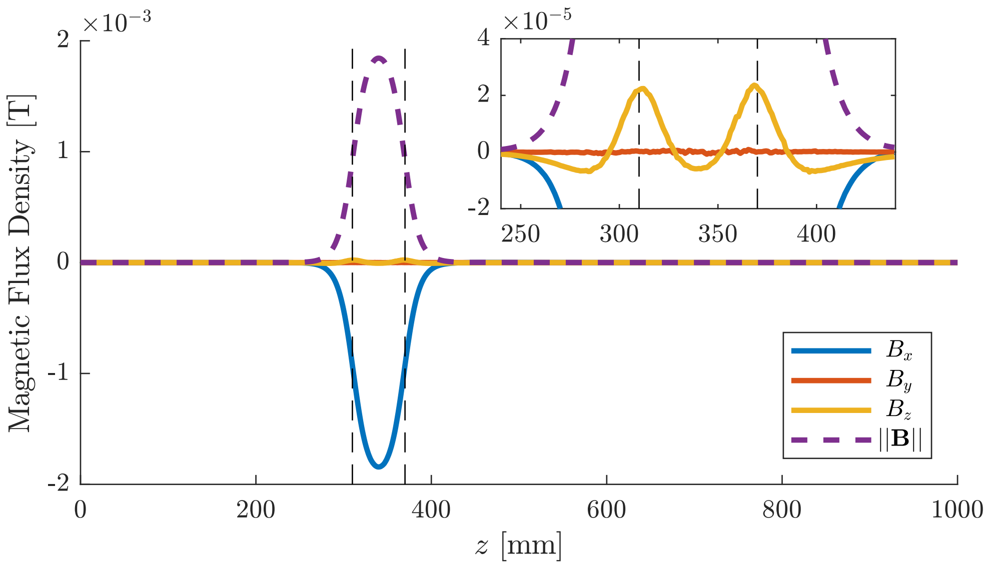

Figure 4.4: Magnetic fields on the z-axis from a single dipole deflection lens. The lens physically extends from the left dashed vertical line to the right.

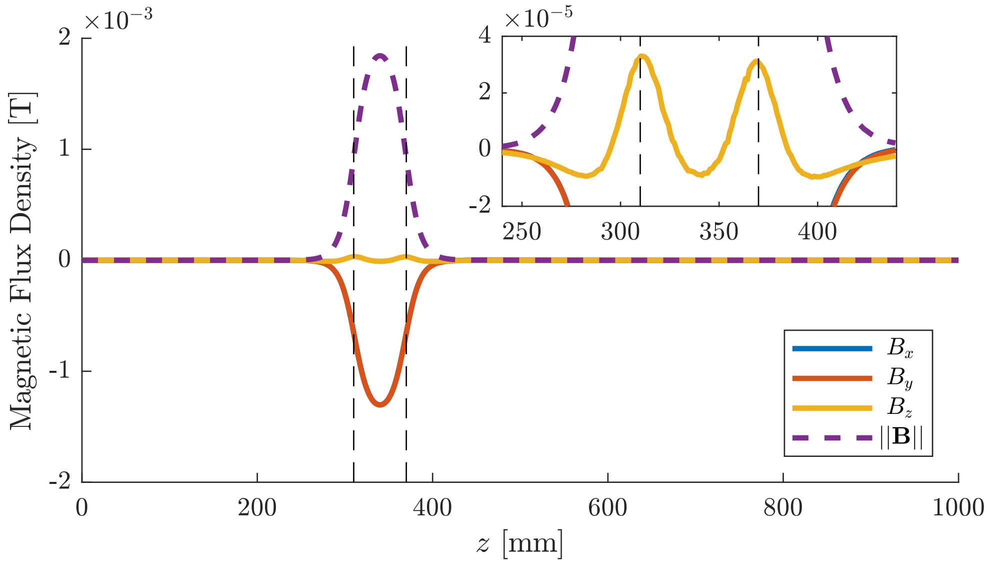

Figure 4.5: Magnetic fields on the z-axis from a double dipole deflection lens. The vertical dashed lines mark the physical boundaries of the lens.

coil. This is shown in figure 4.6 where the magnetic field from sigmators with the symmetry order 4, 6, 8, 12, 16 and 24 are plotted.

4.2 Beam Properties

Once the magnetic fields were solved a study of the charged particle tracing could be made. In the EBM system this is the output of the electron optics and affects the build directly.

4.2.1 Deflected Angles

The relative simplicity of an analytic solution for the beam deflection makes it a suitable candidate for validating the model.

In figure 4.7 the relation between current times number of turns and deflected distances at the wall is shown for an setup with deflection and focus only. The beam entered the model at the origin and traversed the focus lens at 220 mm and the deflection lens at 310 mm until finally hitting the wall at 1000 mm. In one experiment the deflection field originated from only one dipole aligned at a right angle to the desired deflection with current I. In the other experiment the field was solved for two orthogonal dipoles at 45° from the direction of the desired deflection with currents I_x and I_y respectively. In the case with two dipoles the currents were normalized as $\sqrt{I_x^2 + I_y^2} = I$ and the number of turns per coil the same as in the single dipole model.

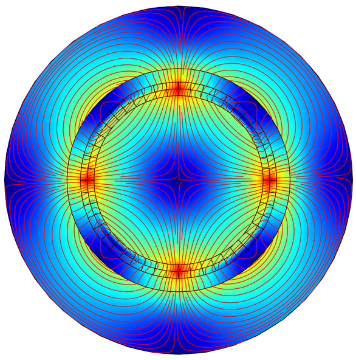

(a) Quadrupole n = 4

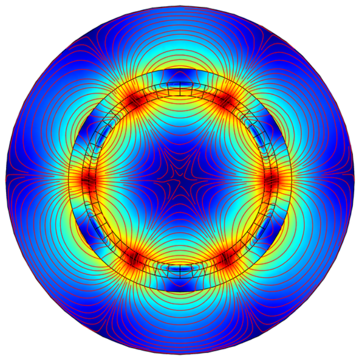

(b) Hexapole n = 6

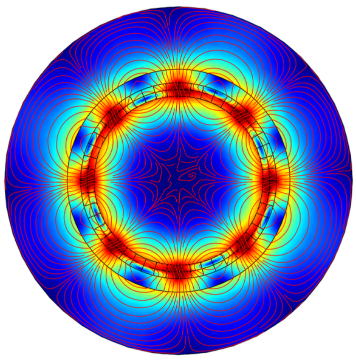

(c) Octupole n = 8

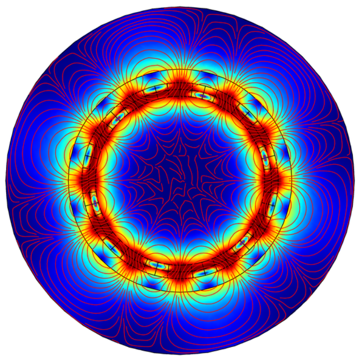

(d) Dodecapole n = 12

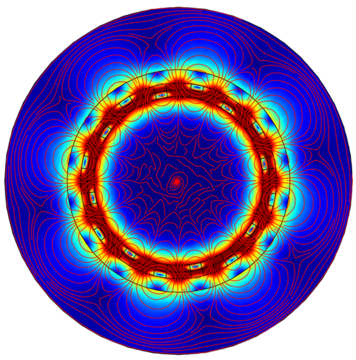

(e) Hexadecapole n = 16

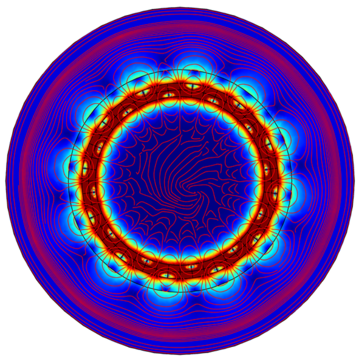

(f) Quadruvigintupole n = 24

Figure 4.6: Plots of magnetic fields resulting from stigmators with symmetry order 4, 6, 8, 12, 16 and 24. The field direction are plotted as red streamlines and the field magnitude is shown as the colored background where red corresponds to the largest magnitude. Note that the magnitude approaches zero at the center of the lens which results in an unstable estimate of the direction of the magnetic field. This effect is particularly noticeable in the stigmators with a higher order of symmetry.

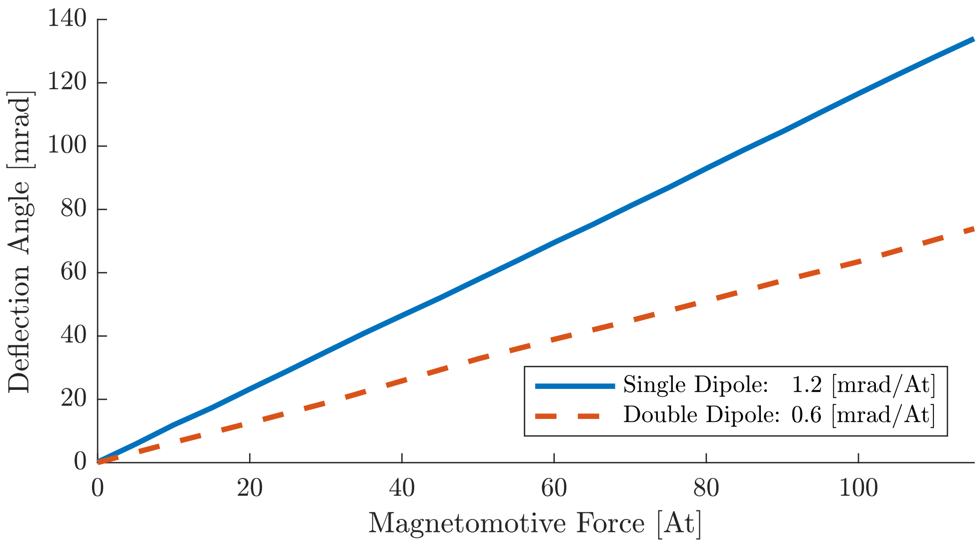

Figure 4.7: Deflection angles from 24 particle tracing simulations of a single dipole deflector and a double dipole respectively. The slopes for the linear least square fits are presented in the legend. The magnetic fields for the two lenses are presented in figure 4.3

4.2.2 Focus Position and Size

A study was made varying the current to the focal lens in a fully deflected system with space charge. The theory presented earlier states that the focusing power should be linear in B_0 for a thin lens neglecting the effect of space charge. In figure 4.8 the effect of space charge as well as size of the lens can be investigated by observing how the behaviour of the beam changes close as it is focused closer to the lens. Another revelation is how the beam size converges for higher magnetomotive forces.

4.2.3 Spectrum of Aberrations due to Deflection and Focusing

Studies were made investigating which aberrations are dominant in EBM. In figure 4.9 a Poincaré section of a beam is shown at its disc of least confusion along with a beam that has been defocused by 15 mm. The densities are shown as the brightness of the color of each electron. One may observe dense rings in the defocused beam and looking at its aberration spectrum in figure 4.10 defocus and higher order spherical aberration is dominant.

A similar study was made by deflecting the beam to the maximum allowed deflection angle. The same well focused reference beam as above was used once more and the densities can be seen in figure 4.11. Looking closer at the deflected beam it is possible to see a slightly elliptic structure. In the aberration spectrum in figure 4.12 this is hard to see due to the shift aberration being so dominant. Neglecting it and normalizing once more we notice how two-fold astigmatism takes the lead.

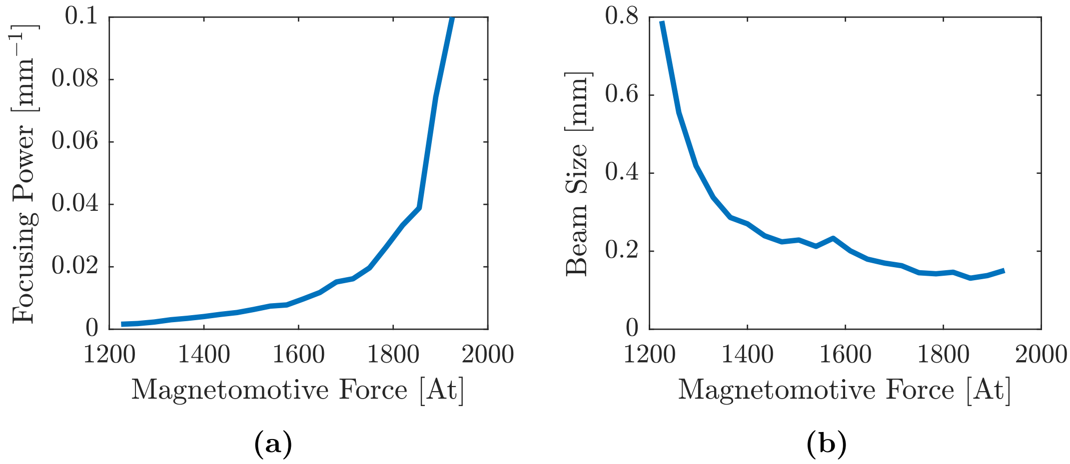

Figure 4.8: **(a)** Focusing power $1/f$ and **(b)** beam size for 24 different settings of the current and number of turns in the focus lens. Focal distance f is measured in mm from the center of the focus lens and the beam size is calculated as the standard deviation of the particles at the focal plane.

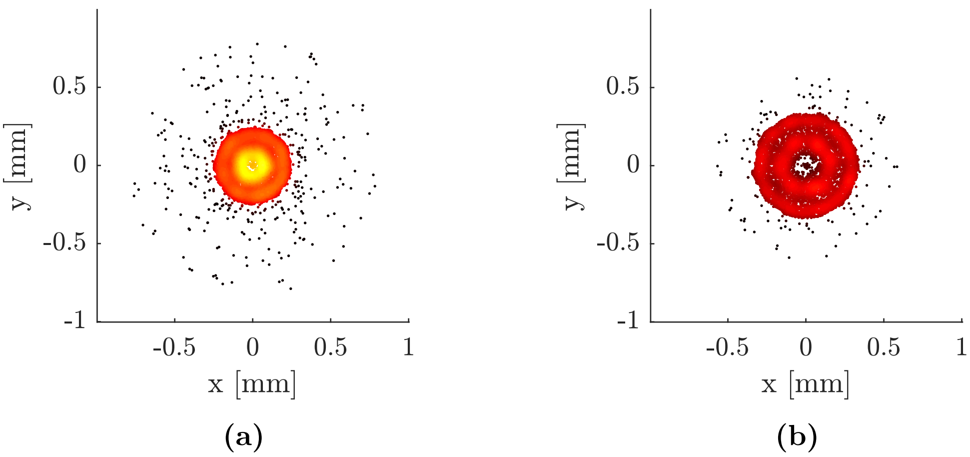

Figure 4.9: Cross section of focused beam of 5000 electrons **(a)** along with beam that has been defocused by 15 mm **(b)**. The density is plotted as the brightness of the colors.

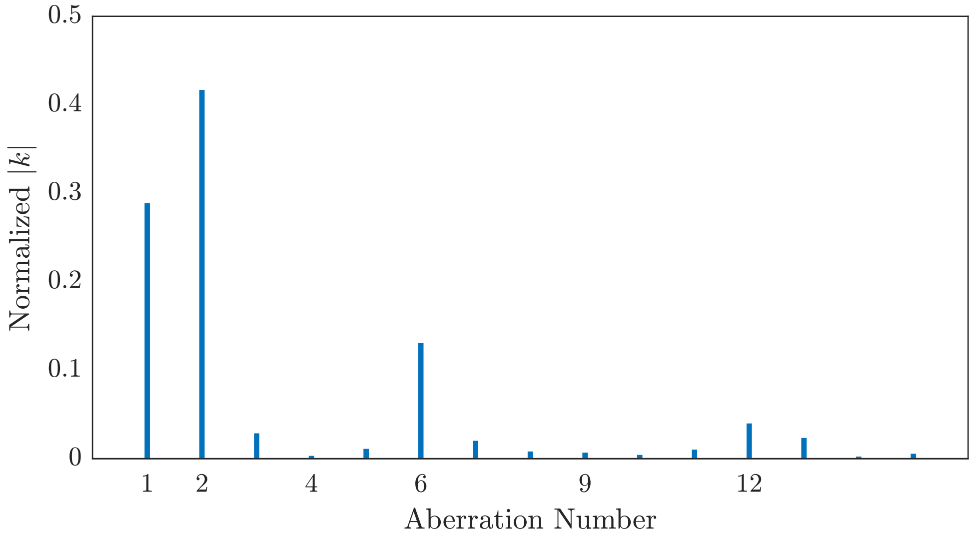

Figure 4.10: Spectrum of aberrations for the beam in figure 4.9b. The basis of the spectrum can read from table 2.1.

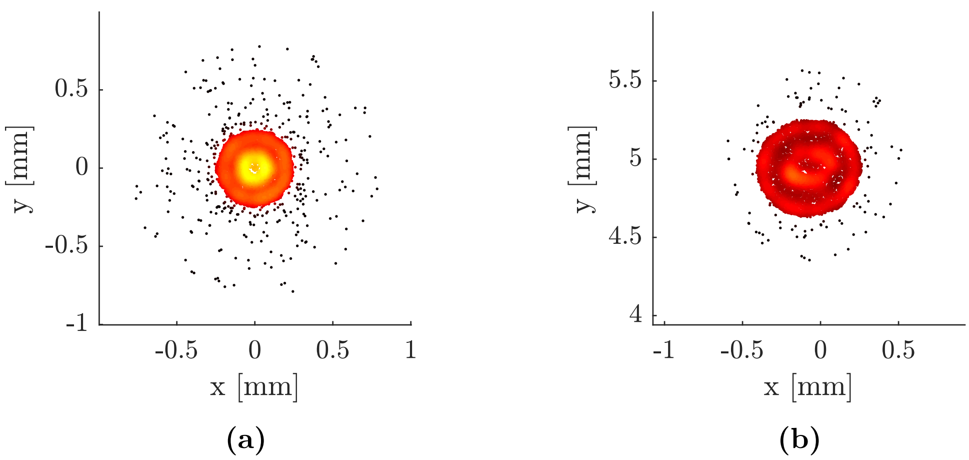

Figure 4.11: Poincaré sections of focused beam of 5000 particles **(a)** and deflected beam with same settings for the focusing lens **(b)**. The densities are shown as the brightness of the points. Notice how **(b)** lies 5 mm away from **(a)**.

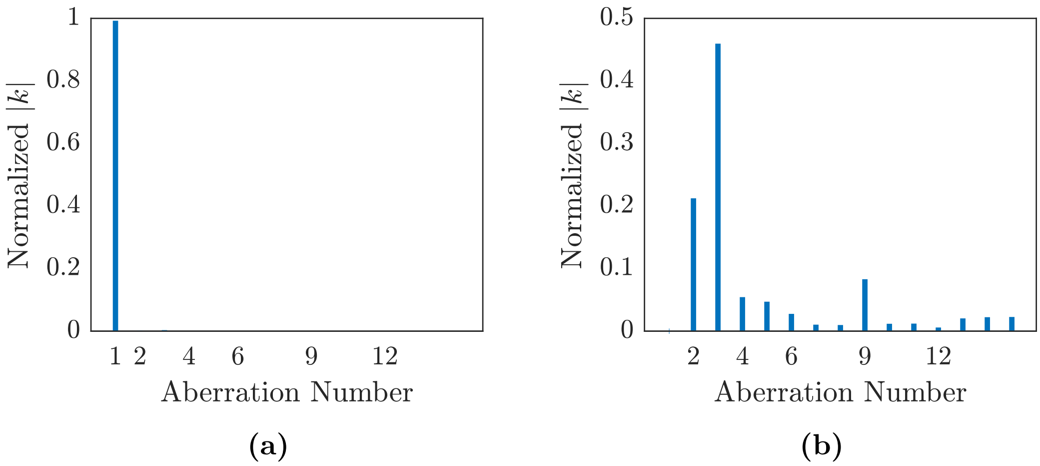

Figure 4.12: Spectrum of aberrations for the beam in figure 4.11b **(a)** and spectrum for the same beam but with the shift coefficient being neglected **(b)**. The basis functions indexed above can be read from table 2.1.

Chapter 5

Conclusion

We have shown how aberrations in an EBM system can be studied and analyzed using a FEM based modeling framework. We have also shown how this model can be used to perform case studies of an EBM system. However, the time constraints imposed by this project has left many of the possible applications of the modeling framework for future studies. There has also been a significant effort to understand the modeling errors and thereby increase the confidence in the results.

5.1 Existing electron optic models

A large part of the available literature review was dedicated to aberration quantification and corrections within electron microscopy. This was mostly due to the fact that no other area of electron optics has seen the same level of development with regards to aberration correction.

However, it is not possible to directly apply the techniques and methods used in electron microscopy to an EBM system. While an EBM system has many superficial similarities with a scanning electron microscope (SEM) there are significant differences which makes the transfer of methods less viable. The angle of the deflection is a factor that results in large differences in the the generation of aberrations. An EBM system can have a deflection angle of hundreds of milliradians compared to a scanning electron microscope where the deflection angle rarely exceeds 50 mrad [21].

Another difference is the beam current where electron microscopes are limited by how much heat that can be deposited into the sample before damaging it. This is in stark contrast to an EBM system where the very purpose is to melt metal powder with a typical maximum beam current on the order of 100 mA. This means that space charge effects will have a comparatively large impact in an EBM system compared to a SEM where the beam current is on the order of 10 µA. These differences are even larger compared to a transmission electron microscope (TEM) which has an ever higher resolution and lower deflection-angle angle than SEM.

The models that are used within electron microscopy therefore have limited use in modeling EBM systems in cases with a comparatively large deflection angle. However, they might be useful in the study of aberrations in an undeflected EBM system.

5.2 The model

Our modeling framework is based on solving the magnetic fields and computing the resulting self-consistent electron trajectories. These trajectories are then used to quantify the aberrations of the system in terms of an aberration spectrum. The current iteration of the modeling framework is configured to be able to model the magnetic fields and beam path in an EBM system.

One of the major challenges with modeling an EBM system is difference in length scales of the features that needs to be modeled. From the scale of the electron beam, which travels 1 m, to the electron density profile used to compute the aberration spectrum, which needs to be defined to lengths on order of 10 µm. The model therefore needs a fine enough mesh to resolve the fine details of the beam while not exceeding the highest number of mesh-elements allowed by the available amount of RAM. Our modeling framework resolves this problem by using a finer mesh in the vicinity of the expected beam trajectory. However, the size of the vacuum that surrounds the EBM system is, despite this, limited by the available amount of RAM.

5.2.1 Speed and Accuracy

Many of the trade-offs made when designing a model based on a finite element method involves trading speed or memory requirement against resolution and accuracy. The scalable nature of the model means that it can be useful even in configurations that requires a very long solution time. We have found that most of our configurations can be solved in about 20 min given that there is sufficient memory. There were times during the project when the solution time was several times longer than it is in the current configuration. The most significant speed-ups came from reducing unnecessary overhead introduced by COMSOL Multiphysics®.

We have performed convergence studies with regards to mesh-element size and number of iterations for the time dependent solver step. While the results from these studies increase our confidence in our model it is necessary to note the importance of performing new convergence studies as the model is developed further.

5.3 Outlook

We have shown a method to analyze the aberration in an EBM system by using data from COMSOL. The uses for this type of analysis range from providing insight into current EBM system to guiding the design of new design and uses for electron optical systems. Our modeling framework is designed to allow for the user to easily extend the functionality.

There are many areas of improvement that were considered but not implemented due to time constraints. We have also considered paths of study to further our understanding of aberrations in an EBM system.

5.3.1 Future improvements of the model

There are many ways in which the modeling framework can be changed in order to improve the functionality and accuracy. Some are related to the user interface while others would focus on the back-end of the model.

There is some need to clarify the scrips used to generate the COMSOL models in order to give the user a better overview of the process. Other related improvements could be to add more options to allow the user to experiment with new types of electron optical designs without having to rebuild large parts of the model. Adding more lenses, changing the order of the lenses and moving them along the optical axis are examples of such studies. Some of the post-processing could also be performed automatically after the computation is completed. This could also reduce the risk of the program crashing due to low amounts of RAM. The model could also be expanded to include factors from the surrounding environment such as stray magnetic fields and fluctuations in the magnetic environment.

5.3.2 Suggested future work

Our modeling framework has laid a foundation for modeling and understanding aberrations in EBM system. However, there are many problem that needs to be solved before the insights gained by our model could be implemented in a physical EBM machine. It has become clear throughout our project that it would be very challenging to mitigate the aberrations without having access to measurements of the actual beam profile in the EBM system. This type of measurements would not only provide a way to verify and improve the models but also function in a feedback based corrections system.

Having a feedback based system becomes even more necessary if the degrees of freedom for the aberration mitigation system were to be increased. A duodecapole has either 12 or 24 independent currents driving it and it would be naive to expect a human operator to be able to perform a calibrations with that number of degrees of freedom. A feedback based system could also benefit from a better understanding of how the aberrations are generated and how they propagate.

While there is a clear transfer of knowledge from a simulation based model to a physical implementation, the opposite type of transfer is not to be underestimated. We would suggest that simple experimental setups of magnetic lenses could be a good way to both verify theories and inform the development of the computer based models. Building a stigmator/deflection combination coil with a high number of poles would be a good first step in this direction. Separating the control of the current in the two coils that make up a pole could also be an interesting starting point for further study.

Bibliography

[1] COMSOL AB. *COMSOL Multiphysics®*. Version 5.3. 2017. URL: `https://comsol.com`.

[2] O. Scherzer. "Über einige Fehler von Elektronenlinsen". In: *Zeitschrift für Physik* 101.9 (1936), pp. 593–603. ISSN: 0044-3328. DOI: `10.1007/BF01349606`.

[3] Runze Huang et al. "Energy and emissions saving potential of additive manufacturing: the case of lightweight aircraft components". In: *Journal of Cleaner Production* 135 (2016), pp. 1559–1570. ISSN: 0959-6526. DOI: `10.1016/j.jclepro.2015.04.109`.

[4] P.W. Hawkes and E. Kasper. *Principles of Electron Optics*. Ed. by P.W. Hawkes and E. Kasper. Vol. 1. San Diego: Academic Press, 1996, pp. 3–14. ISBN: 978-0-12-333340-7. DOI: `10.1016/B978-012333340-7/50180-0`.

[5] Ernst Ruska. "The development of the electron microscope and of electron microscopy". In: *Rev. Mod. Phys.* 59 (3 July 1987), pp. 627–638. DOI: `10.1103/RevModPhys.59.627`.

[6] P. W. Hawkes. "Aberration correction past and present". In: *Philosophical Transactions of the Royal Society of London A* 367.1903 (2009), pp. 3637–3664. ISSN: 1364-503X. DOI: `10.1098/rsta.2009.0004`.

[7] Maximilian Haider et al. "Towards 0.1 nm resolution with the first spherically corrected transmission electron microscope". In: *Journal of Electron Microscopy* 47.5 (1998), p. 395. DOI: `10.1093/oxfordjournals.jmicro.a023610`.

[8] Harald Rose. *Geometrical Charged-Particle Optics*. 2nd 2012. Vol. 142. Springer Berlin Heidelberg, 2012. ISBN: 9783642321184.

[9] R. F. Egerton. *Physical Principles of Electron Microscopy: An Introduction to TEM, SEM, and AEM*. 2nd 2016. Cham: Springer International Publishing, 2016. ISBN: 9783319398778.

[10] A. Glindemann et al. "Adaptive Optics on Large Telescopes". In: *Experimental Astronomy* 10.1 (2000), pp. 5–47. ISSN: 1572-9508. DOI: `10.1023/A:1008116831367`.

[11] Makoto Saika et al. "Four discriminant models for detecting keratoconus pattern using Zernike coefficients of corneal aberrations". In: *Japanese Journal of Ophthalmology* 57.6 (2013), pp. 503–509. ISSN: 1613-2246. DOI: `10.1007/s10384-013-0269-1`.

[12] R. Brydson. *Aberration-Corrected Analytical Transmission Electron Microscopy.* RMS - Royal Microscopical Society. Wiley, 2011. ISBN: 9781119979906.

[13] Tristan Needham. *Visual complex analysis.* English. 1. paperback (with corrections). Oxford: Clarendon, 1998. ISBN: 9780198534464.

[14] Rolf Erni. *Aberration-corrected imaging in transmission electron microscopy: An introduction.* World Scientific Publishing Co Inc, 2015. ISBN: 9781848165366.

[15] David C. Joy, Alton D. Romig, and Joseph I. Goldstein. *Principles of Analytical Electron Microscopy.* Boston, MA: Springer US, 1986. ISBN: 9781489920393.

[16] Anders Logg. *FEniCS Course, Lecture 0: Introduction to FEM.* Apr. 2017. URL: `https://fenicsproject.org/pub/course/lectures/2017-nordic-phdcourse`.

[17] David K. Cheng. *Field and wave electromagnetics.* English. 2. Reading, Mass: Addison-Wesley Pub. Co, 1989. ISBN: 9780201128192.

[18] Jianming Jin. *The finite element method in electromagnetics.* 3rd. Hoboken, NJ: John Wiley & Sons, 2014. ISBN: 9781118571361.

[19] J. C. Nedelec. "Mixed finite elements in $\mathbb{R}^3$". In: *Numerische Mathematik* 35.3 (1980), pp. 315–341. ISSN: 0945-3245. DOI: `10.1007/BF01396415`.

[20] O.L. Krivanek, N. Dellby, and A.R. Lupini. "Towards sub-Å electron beams". In: *Ultramicroscopy* 78.1–4 (1999), pp. 1–11. ISSN: 0304-3991. DOI: `10.1016/S0304-3991(99)00013-3`.

[21] Ludwig Reimer. *Scanning Electron Microscopy: Physics of Image Formation and Microanalysis.* English. Second Completely Revis and Updat. Vol. 45. Springer Berlin Heidelberg, 1998. ISBN: 9783642083723. DOI: `10.1007/978-3-540-38967-5`.

[22] John D. Jackson. *Classical electrodynamics.* English. New York, 1962. ISBN: 9789900185239.

Appendix A

Error Estimation

Solving continuous infinite dimensional problems on a computer always results in errors. In order interpret the numerical solutions one must know the size of the errors. In this section we quantify the numerical errors.

A.0.1 Magnetic Fields

One way of quantifying the errors is through studying how the solution depends on the size of the discretization. The standard procedure is to parametrize the size of the largest element of the mesh in a mesh refinement factor. Here we label it mesh element size factor because the results in the body of this thesis have been obtained with finest mesh available to our hardware. The convergence studies were instead made through coarsening the mesh with 1 being the finest mesh and 5 being the coarsest.

Here we present the results from a mesh coarsening study on a system with a focusing lens and with maximum deflection.

We define a error measure at position $\mathbf{r}_i$ for the magnetic fields presented is

$$\delta(\mathbf{r}_i) = \sqrt{(B_x - B_x')^2 + (B_y - B_y')^2 + (B_y - B_y')^2}. \tag{A.1}$$

Here the primed fields are the fields under trial and the unprimed fields are the components of the reference field. To compact this we take the l^2 norm over all $\mathbf{r}_i$ as

$$\epsilon = \sqrt{\sum_i \delta(r_i)^2}. \tag{A.2}$$

In figure A.1 the volume residual error is shown for different orders of magnitude of the number of degrees of freedom up to what was normally used in the simulations.

In practice the error mattered the most on the on the z-axis, why the l^2 norm is for the majority of the results only taken in one dimension. In figure A.2 $\delta(\mathbf{r}_i) = \delta(z_i)$ is shown where the reference solution is compared with a solution with a five times coarser mesh. In figure A.3 the l^2 measure ϵ is shown for solutions with varying mesh element size factors.

A universal measure for the physicality of the solutions how well it preserves energy. The magnetostatic energy in a volume Ω is defined as [22]

$$W = \int_\Omega \mathbf{H} \cdot \mathbf{B} \, \mathrm{d}^3\mathbf{r}\,. \tag{A.3}$$

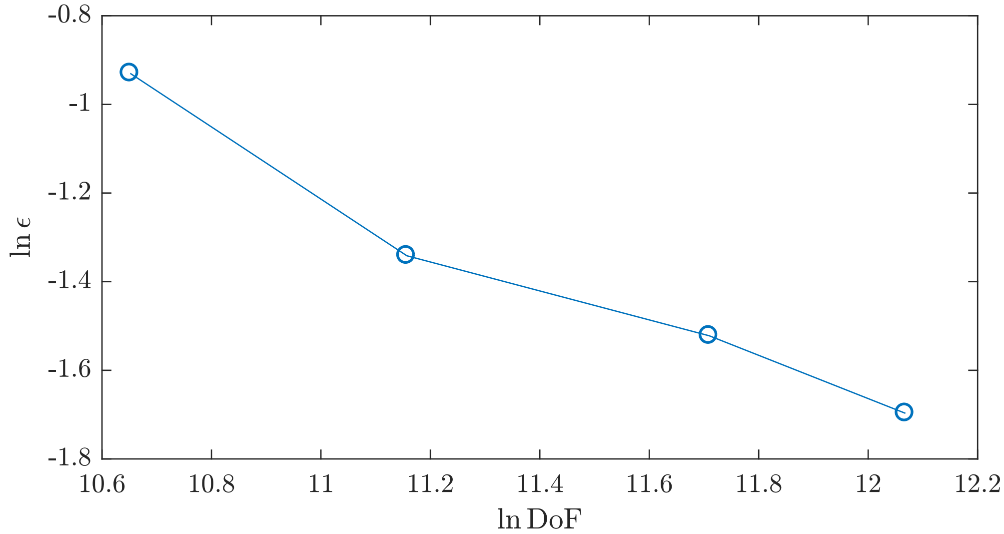

Figure A.1: Absolute l^2 volume summed residuals to solution with 283377 DoFs ($e^{12.6}$).

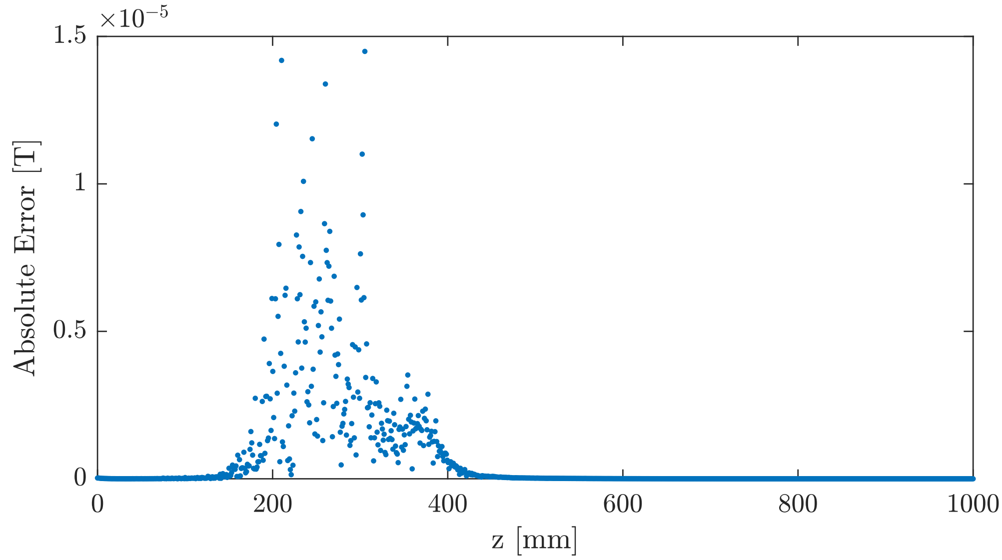

Figure A.2: Magnitude of the error vector for the B field on the z-axis. The solutions being compared are the ones with mesh refinement factor 1/5 to 1.

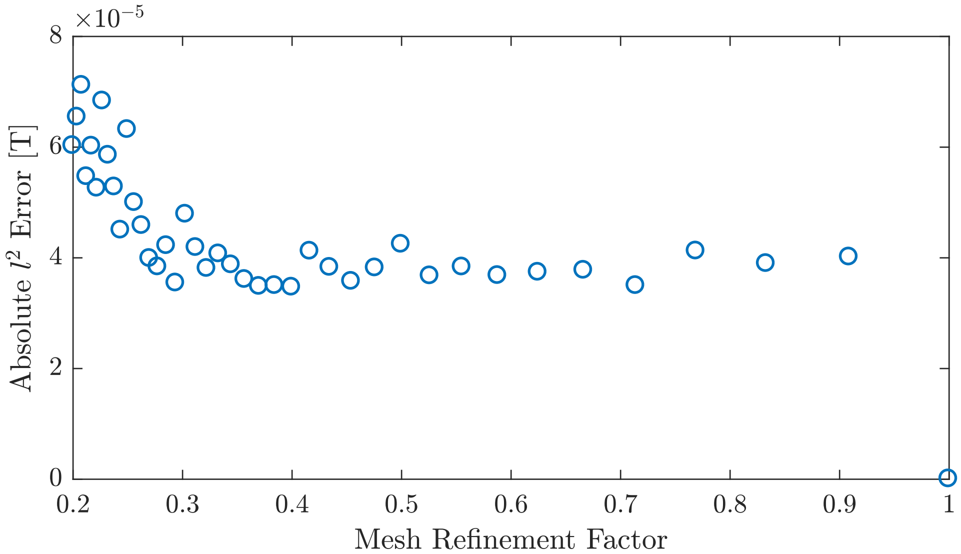

Figure A.3: l^2 norm of the magnitude of the error vectors for the $\mathbf{B}$ field on the z-axis. Deviations calculated from mesh element size factor 1.

The total magnetic energy was calculated for different mesh sizes. The error

$$\epsilon = |W - W'| \tag{A.4}$$

is shown in figure A.4.

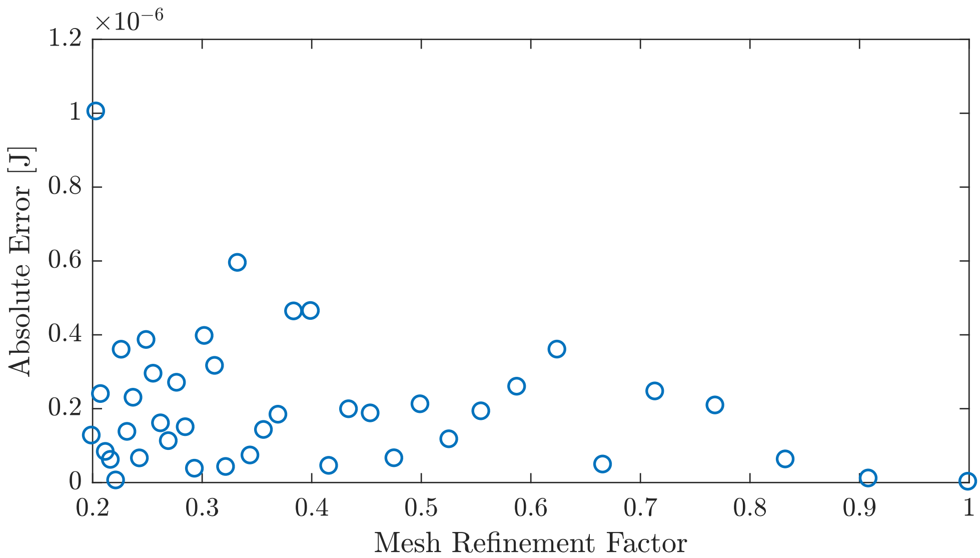

Figure A.4: Absolute value of deviations in total magnetic energy relative to the model with mesh element size factor 1.